

Inverse Entropic Optimal Transport Solves Semi-supervised Learning via Data Likelihood Maximization

Mikhail Pershiyanov¹ Arip Asadulaev^{2,3} Nikita Andreev Nikita Starodubcev⁴ Dmitry Baranchuk⁴
Anastasis Kratsios^{5,6} Evgeny Burnaev^{1,2} Alexander Korotin^{1,2}

Abstract

Learning conditional distributions $\pi^*(\cdot|x)$ is a central problem in machine learning, which is typically approached via supervised methods with paired data $(x, y) \sim \pi^*$. However, acquiring paired data samples is often challenging, especially in problems such as domain translation. This necessitates the development of *semi-supervised* models that utilize both limited paired data and additional unpaired i.i.d. samples $x \sim \pi_x^*$ and $y \sim \pi_y^*$ from the marginal distributions. The usage of such combined data is complex and often relies on heuristic approaches. To tackle this issue, we propose a new learning paradigm that integrates both paired and unpaired data **seamlessly** using data likelihood maximization techniques. We demonstrate that our approach also connects intriguingly with inverse entropic optimal transport (OT). This finding allows us to apply recent advances in computational OT to establish a **light** learning algorithm to get $\pi^*(\cdot|x)$. In addition, we derive the universal approximation property demonstrating that our approach can theoretically recover true conditional distributions with arbitrarily small error. Furthermore, we demonstrate through empirical tests that our method effectively learns conditional distributions using paired and unpaired data simultaneously.

1. Introduction

Recovering conditional distributions $\pi^*(y|x)$ from data is one of the fundamental problems in machine learning, which appears both in predictive and generative modeling. In

¹Skolkovo Institute of Science and Technology, Moscow, Russia. ²Artificial Intelligence Research Institute, Moscow, Russia. ³ITMO University, Saint Petersburg, Russia. ⁴Yandex Research, Moscow, Russia. ⁵Vector Institute, Toronto, Canada. ⁶McMaster University, Hamilton, Canada. Correspondence to: Mikhail Pershiyanov <m.pershiyanov@skoltech.ru>.

Preprint.

predictive modeling, the standard examples of such tasks are the classification, where $x \in \mathbb{R}^{D_x}$ is a feature vector and $y \in \{0, 1, \dots, K\}$ is a class label, and regression, in which case x is also a feature vector and $y \in \mathbb{R}$ is a real number. In generative modeling, both x and y are feature vectors in $\mathbb{R}^{D_x}, \mathbb{R}^{D_y}$, respectively, representing complex objects, and the goal is to find a transformation between them.

In our paper, we focus on the case when x and y are multi-dimensional real-valued vectors and the true joint data distribution $\pi^*(x, y)$ is a continuous data distribution on $\mathbb{R}^{D_x} \times \mathbb{R}^{D_y}$, i.e., we exclude the problems when, e.g., y is a discrete object such as the class label. That is, the scope of our paper is the multi-dimensional probabilistic regression problems, which can be referred to as **domain translation** problems, as usually x and y are feature vectors representing data from different domains. In turn, the goal is to make a (probabilistic) prediction, where for a new object x_{new} from the input domain, we aim to predict the corresponding data y_{new} from the target domain, according to the conditional distribution $\pi^*(y|x)$.

It is very natural that to learn the conditional distributions $\pi^*(y|x)$ of data one requires input-target data pairs $(x, y) \sim \pi^*$, where π^* is the true joint distribution of data. In this case, $\pi^*(y|x)$ can be modeled via standard supervised learning approaches starting from a simple regression and ending with conditional generative models (Mirza & Osindero, 2014; Winkler et al., 2019). However, acquiring paired data may be costly, while getting unpaired samples $x \sim \pi_x^*$ or $y \sim \pi_y^*$ from two domains may be much easier and cheaper. This fact inspired the development of unsupervised (or unpaired) learning methods, e.g., (Zhu et al., 2017) among many others, which aim to somehow reconstruct the dependencies $\pi^*(y|x)$ with access to unpaired data only.

While both paired (supervised) and unpaired (unsupervised) domain translation approaches are being extremely well developed nowadays, surprisingly, the semi-supervised setup when **both** paired and unpaired data is available is much less explored. This is due to the **challenge of designing learning objective** (loss) which can simultaneously take into account both paired and unpaired data. For example, one potential strategy here is to heuristically combine typ-

ical paired and unpaired losses. However, such a strategy leads to complex training objectives, see (Tripathy et al., 2019, §3.5), (Jin et al., 2019, §3.3), (Yang & Chen, 2020, §C), (Vasluianu et al., 2021, §3), (Panda et al., 2023, Eq. 8), (Tang et al., 2024, Eq. 8), (Theodoropoulos et al., 2024, §3.2), (Gu et al., 2023, §3). However, as we show in §5.1, such objectives fail to capture **true** conditional distribution even for simple cast with $D_x = D_y = 2$. Therefore, it is reasonable to raise a question: *is it possible to design a simple loss to learn $\pi^*(y|x)$ which **naturally** takes into account both paired and unpaired data?*

In our paper, we positively answer the above-raised question. Our **main contributions** can be summarized as follows:

1. We introduce a novel loss function designed to facilitate the learning of conditional distributions $\pi^*(\cdot|x)$ using both paired and unpaired training samples derived from π^* (§3.1). This loss function is based on the well-established principle of likelihood maximization. Our approach’s notable advantage lies in its capacity to support end-to-end learning, thereby *seamlessly* integrating both paired and unpaired data into the training process.
2. We demonstrate the theoretical equivalence between our proposed loss function and the *inverse entropic optimal transport* problem (§3.2). This finding enables to leverage established computational OT methods to address challenges encountered in semi-supervised learning.
3. Building upon recent advancements in the field of computational optimal transport, we provide a *light and end-to-end* algorithm exploiting the Gaussian mixture parameterization specifically tailored to optimize our proposed likelihood-based loss function (in §3.3).
4. We prove that our proposed parameterization satisfies the universal approximation property, which theoretically allows our algorithm to recover π^* arbitrarily well (§3.4).

Our empirical validation in §5 shows the impact of both unpaired and paired data on overall performance. In particular, our findings reveal that conditional distributions $\pi^*(\cdot|x)$ can be effectively learned even with a modest quantity of paired data $(x, y) \sim \pi^*$, provided that a sufficient amount of auxiliary unpaired data $x \sim \pi_x^*, y \sim \pi_y^*$ is available.

Notations. Throughout the paper, \mathcal{X} and \mathcal{Y} represent Euclidean spaces, equipped with the standard norm $\|\cdot\|$, induced by the inner product $\langle \cdot, \cdot \rangle$, i.e., $\mathcal{X} \stackrel{\text{def}}{=} \mathbb{R}^{D_x}$ and $\mathcal{Y} \stackrel{\text{def}}{=} \mathbb{R}^{D_y}$. The set of absolutely continuous probability distributions on \mathcal{X} is denoted by $\mathcal{P}_{ac}(\mathcal{X})$. For simplicity, we use the same notation for both the distributions and their corresponding probability density functions. The joint probability distribution over $\mathcal{X} \times \mathcal{Y}$ is denoted by π with corresponding marginals π_x and π_y . The set of joint distributions with given marginals α and β is represented by $\Pi(\alpha, \beta)$. We use $\pi(\cdot|x)$ for the conditional distribution, while $\pi(y|x)$ repre-

sents the conditional density at a specific point y . The differential entropy is given by $H(\beta) = - \int_{\mathcal{Y}} \beta(y) \log \beta(y) dy$.

2. Background

First, we recall the formulation of the domain translation problem (§2.1). We remind the difference between its paired, unpaired, and semi-supervised setups. Next, we recall the basic concepts of the inverse entropic optimal transport, which are relevant to our paper (§2.2).

2.1. Domain Translation Problems

The goal of *domain translation* (DT) task is to transform data samples from the source domain to the target domain while maintaining the essential content or structure. This approach is widely used in applications like computer vision (Zhu et al., 2017; Lin et al., 2018; Peng et al., 2023), natural language processing (Jiang et al., 2021; Morishita et al., 2022), and audio processing (Du et al., 2022), etc. Domain translation task setups can be classified into supervised (paired), unsupervised (unpaired), and semi-supervised approaches based on the data used for training (Figure 1).

Supervised domain translation relies on matched examples from both the source and target domains, where each input corresponds to a specific output, enabling direct supervision during the learning process. Formally, this setup assumes access to a set of P empirical pairs $XY_{\text{paired}} \stackrel{\text{def}}{=} \{(x_1, y_1), \dots, (x_P, y_P)\} \sim \pi^*$ from some unknown joint distribution. The goal here is to recover the conditional distributions $\pi^*(\cdot|x)$ to generate samples $y|x_{\text{new}}$ for new inputs x_{new} that are not present in the training data. While this task is relatively straightforward to solve, obtaining such paired training datasets can be challenging, as it often involves significant time, cost, and effort.

Unsupervised domain translation, in contrast, does not require direct correspondences between the source and target domains (Zhu et al., 2017, Figure 2). Instead, it involves learning to translate between domains using unpaired data, which offers greater flexibility but demands advanced techniques to achieve accurate translation. Formally, we are given Q unpaired empirical samples $X_{\text{unpaired}} \stackrel{\text{def}}{=} \{x_1, \dots, x_Q\} \sim \pi_x^*$ from the source distribution and R unpaired samples $Y_{\text{unpaired}} \stackrel{\text{def}}{=} \{y_1, \dots, y_R\} \sim \pi_y^*$ from the target distribution. Our objective is to learn the conditional distributions $\pi^*(\cdot|x)$ of the unknown joint distribution π^* , whose marginals are π_x^*, π_y^* , respectively. Clearly, the primary challenge in unpaired setup is that the task is inherently ill-posed, leading to multiple potential solutions, many of which may be ambiguous or even not meaningful (Morikov et al., 2020). Ensuring the translation’s accuracy and relevance requires careful consideration of constraints and regularization strategies to guide the learning process (Yuan

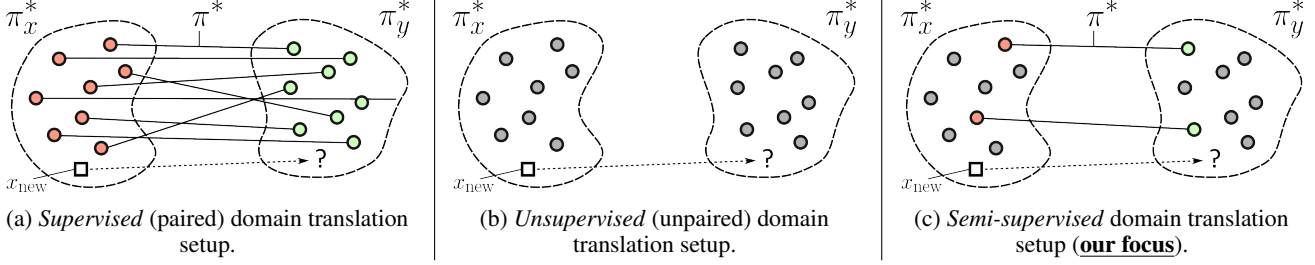


Figure 1. Visualization of domain translation setups. Red and green colors indicated paired training data XY_{paired} , while grey color indicates the unpaired training data $X_{\text{unpaired}}, Y_{\text{unpaired}}$.

et al., 2018). Overall, the unpaired setup is very important because of large amounts of unpaired data in the wild.

Semi-supervised domain translation integrates both paired and unpaired data to enhance the translation process (Tripathy et al., 2019; Jiang et al., 2023). This approach leverages the precision of paired data to guide the model while exploiting the abundance of unpaired data to improve performance and generalization. Formally, the setup assumes access to paired data $XY_{\text{paired}} \sim \pi^*$ as well as additional unpaired samples $X_{\text{unpaired}} \sim \pi_x^*$ and $Y_{\text{unpaired}} \sim \pi_y^*$. Note that paired samples can also be used in an unpaired manner. By convention, we assume $P \leq Q, R$, where the first P unpaired samples are identical to the paired ones. The goal remains to learn the true conditional mapping $\pi^*(\cdot|x)$ using the available data.

2.2. Optimal Transport (OT)

The foundations of optimal transport are detailed in books (Villani et al., 2009; Santambrogio, 2015; Peyré et al., 2019).

Entropic OT (Cuturi, 2013; Genevay, 2019). Consider source $\alpha \in \mathcal{P}_{\text{ac}}(\mathcal{X})$ and target $\beta \in \mathcal{P}_{\text{ac}}(\mathcal{Y})$ distributions. Let $c^* : \mathcal{X} \times \mathcal{Y} \rightarrow \mathbb{R}$ be a cost function. The *entropic* optimal transport problem between distributions α and β is then defined as follows:

$$\text{OT}_{c^*, \varepsilon}(\alpha, \beta) \stackrel{\text{def}}{=} \min_{\pi \in \Pi(\alpha, \beta)} \mathbb{E}_{x, y \sim \pi} [c^*(x, y)] - \varepsilon \mathbb{E}_{x \sim \alpha} \text{H}(\pi(\cdot|x)), \quad (1)$$

where $\varepsilon > 0$ is the regularization parameter. Setting $\varepsilon = 0$ recovers the classic OT formulation (Villani et al., 2009) originally proposed by (Kantorovich, 1942). Under mild assumptions, there exists a unique transport plan $\pi^* \in \Pi(\alpha, \beta)$ that minimizes the objective function defined in (1). This plan is referred to as the *entropic optimal transport plan*.

We note that in the literature, the entropy regularization term in (1) is usually $-\varepsilon \text{H}(\pi)$ or $+\varepsilon \text{KL}(\pi || \alpha \times \beta)$. However, these forms are equivalent up to constants, see discussion in (Mokrov et al., 2024, §2) or (Gushchin et al., 2023, §1). In our paper, we work only with formulation (1), which is also known as the *weak* form of the entropic OT, see (Gozlan et al., 2017; Backhoff-Veraguas et al., 2019; Backhoff-Veraguas & Pammer, 2022).

Dual formulation. With mild assumptions on c^*, α, β , the following dual OT formulation holds:

$$\text{OT}_{c^*, \varepsilon}(\alpha, \beta) = \sup_f \left\{ \mathbb{E}_{x \sim \alpha} f^{c^*}(x) + \mathbb{E}_{y \sim \beta} f(y) \right\}, \quad (2)$$

where f ranges over a certain subset of continuous functions (dual potentials) with mild assumptions on their boundness, see (Backhoff-Veraguas & Pammer, 2022, Eq. 3.3) for details. The term f^{c^*} represents the so-called *weak entropic c^* -transform* of f , defined as:

$$f^{c^*}(x) \stackrel{\text{def}}{=} \min_{\beta \in \mathcal{P}(\mathcal{Y})} \left\{ \mathbb{E}_{y \sim \beta} [c^*(x, y)] - \varepsilon \text{H}(\beta) - \mathbb{E}_{y \sim \beta} f(y) \right\}.$$

It has closed-form (Mokrov et al., 2024, Eq. 14) given by:

$$f^{c^*}(x) = -\varepsilon \log \int_{\mathcal{Y}} \exp \left(\frac{f(y) - c^*(x, y)}{\varepsilon} \right) dy. \quad (3)$$

Inverse entropic OT. The forward OT problem (1) focuses on determining the OT plan π^* given a predefined cost function c^* . In contrast, the inverse problem provides the learner with a joint distribution π^* and requires finding a cost function c^* such that π^* becomes the OT plan between its marginals, π_x^* and π_y^* . This setup leads to the formulation of the *inverse entropic OT* problem, which can be expressed as the following minimization problem:

$$c^* \in \arg \min_c \left[\underbrace{\mathbb{E}_{x, y \sim \pi^*} [c(x, y)]}_{\geq \text{OT}_{c, \varepsilon}(\pi_x^*, \pi_y^*)} - \overbrace{\varepsilon \mathbb{E}_{x \sim \pi_x^*} \text{H}(\pi^*(\cdot|x))}_{\text{not depend on } c} - \text{OT}_{c, \varepsilon}(\pi_x^*, \pi_y^*) \right], \quad (4)$$

where c skims through measurable functions $\mathcal{X} \times \mathcal{Y} \rightarrow \mathbb{R}$. The expression within the parentheses denotes the entropic transport cost of the plan π^* in relation to the cost c between the marginals π_x^* and π_y^* , thus ensuring that it is always greater than or equal to the optimal cost $\text{OT}_{c, \varepsilon}(\pi_x^*, \pi_y^*)$. Consequently, the minimum achievable value for the entire objective is zero, which occurs only when π^* corresponds to the optimal transport plan for the selected cost c^* . Here, the term $-\varepsilon \mathbb{E}_{x \sim \pi_x^*} \text{H}(\pi^*(\cdot|x))$ can be omitted, as it does not depend on c . Additionally

- Unlike the forward OT problem (1), the entropic regularization parameter $\varepsilon > 0$ here plays no significant role. Indeed, by substituting $c(x, y) = \frac{\varepsilon}{\varepsilon'} c'(x, y)$ and multiplying the entire objective (4) by $\frac{\varepsilon'}{\varepsilon}$, one gets the inverse OT problem for ε' . Hence, the problems associated with different ε are equivalent up to the change of variables, which is not the case for the forward OT (1).
- The inverse problem admits *several* possible solutions c^* . For example, $c^*(x, y) = -\varepsilon \log \pi^*(x, y)$ provides the minimum, which can be verified through direct substitution. Similarly, cost functions of the form $c^*(x, y) = -\varepsilon \log \pi^*(x, y) + u(x) + v(y)$ are also feasible, as adding terms dependent only on x or y does not alter the OT plan. In particular, when $u(x) = \varepsilon \log \pi_x^*(x)$ and $v(y) = 0$, one gets $c^*(x, y) = -\varepsilon \log \pi^*(y|x)$.

In practice, the joint distribution π^* is typically available only through empirical samples, meaning that its density is often unknown. As a result, specific solutions such as $c^*(x, y) = -\varepsilon \log \pi^*(x, y)$ or $-\varepsilon \log \pi^*(y|x)$ cannot be directly utilized. Consequently, it becomes necessary to develop parametric estimators π^θ to approximate them.

3. Semi-supervised Domain Translation via Inverse Entropic Optimal Transport

In §3.1, we develop our proposed loss function that seamlessly integrates both paired and unpaired data samples. In §3.2, we demonstrate that derived loss is inherently linked to the inverse entropic optimal transport problem (4). In §3.3, we introduce lightweight parametrization to overcome challenges associated with optimizing the loss function. All our proofs can be found in Appendix D.

3.1. Loss Derivation

Part I. Data likelihood maximization and its limitation.

Our goal is to approximate the true distribution π^* by some parametric model π^θ , where θ represents the parameters of the model. To achieve this, we would like to employ the standard KL-divergence minimization framework, also known as data likelihood maximization. Namely, we minimize

$$\text{KL}(\pi^* \parallel \pi^\theta) = \mathbb{E}_{x, y \sim \pi^*} \log \frac{\pi_x^*(x) \pi^*(y|x)}{\pi_x^\theta(x) \pi^\theta(y|x)} = \quad (5)$$

$$\mathbb{E}_{x \sim \pi_x^*} \log \frac{\pi_x^*(x)}{\pi_x^\theta(x)} + \mathbb{E}_{x, y \sim \pi^*} \log \frac{\pi^*(y|x)}{\pi^\theta(y|x)} = \quad (6)$$

$$\text{KL}(\pi_x^* \parallel \pi_x^\theta) + \mathbb{E}_{x \sim \pi_x^*} \mathbb{E}_{y \sim \pi^*(\cdot|x)} \log \frac{\pi^*(y|x)}{\pi^\theta(y|x)} = \quad (7)$$

$$\underbrace{\text{KL}(\pi_x^* \parallel \pi_x^\theta)}_{\text{Marginal}} + \underbrace{\mathbb{E}_{x \sim \pi_x^*} \text{KL}(\pi^*(\cdot|x) \parallel \pi^\theta(\cdot|x))}_{\text{Conditional}}. \quad (8)$$

It is clear that objective (8) splits into two **independent** components: the *marginal* and the *conditional* matching terms. Our focus will be on the conditional component $\pi^\theta(\cdot|x)$, as

it is the necessary part for the domain translation. Note that the marginal part π_x^θ is not actually needed. The conditional part of (8) can further be divided into the following terms:

$$\mathbb{E}_{x \sim \pi_x^*} \mathbb{E}_{y \sim \pi^*(\cdot|x)} [\log \pi^*(y|x) - \log \pi^\theta(y|x)] = \quad (9)$$

$$-\mathbb{E}_{x \sim \pi_x^*} \text{H}(\pi^*(\cdot|x)) - \mathbb{E}_{x, y \sim \pi^*} \log \pi^\theta(y|x).$$

The first term is independent of θ , so we obtain the following minimization objective:

$$\mathcal{L}(\theta) \stackrel{\text{def}}{=} -\mathbb{E}_{x, y \sim \pi^*} \log \pi^\theta(y|x). \quad (10)$$

It is important to note that minimizing (10) is equivalent to maximizing the conditional likelihood, a strategy utilized in conditional normalizing flows (Papamakarios et al., 2021, CNF). However, a major limitation of this approach is its reliance solely on paired data from π^* , which can be difficult to obtain in real-world scenarios. In the following section, we modify this strategy to incorporate available unpaired data within a semi-supervised learning setup (see §2.1).

Part II. Solving the limitations via a smart parameterization. To address the above-mentioned issue and leverage unpaired data, we first use Gibbs-Boltzmann distribution (LeCun et al., 2006) density parametrization:

$$\pi^\theta(y|x) \stackrel{\text{def}}{=} \frac{\exp(-E^\theta(y|x))}{Z^\theta(x)}, \quad (11)$$

where $E^\theta(\cdot|x) : \mathcal{Y} \rightarrow \mathbb{R}$ is *the Energy function*, and $Z^\theta(x) \stackrel{\text{def}}{=} \int_{\mathcal{Y}} \exp(-E^\theta(y|x)) dy$ is the normalization constant. Substituting (11) into (10), we obtain:

$$\mathcal{L}(\theta) = \mathbb{E}_{x, y \sim \pi^*} E^\theta(y|x) + \mathbb{E}_{x \sim \pi_x^*} \log Z^\theta(x). \quad (12)$$

This objective already provides an opportunity to exploit the unpaired samples from the marginal distribution π_x^* to learn the conditional distributions $\pi^\theta(\cdot|x) \approx \pi^*(\cdot|x)$. Namely, it helps to estimate the part of the objective related to the normalization constant Z^θ . To incorporate independent samples from the second marginal distribution π_y^* , it is crucial to adopt a parametrization that separates the term in the energy function $E^\theta(y|x)$ that depends only on y . Thus, we propose:

$$E^\theta(y|x) \stackrel{\text{def}}{=} \frac{c^\theta(x, y) - f^\theta(y)}{\varepsilon}. \quad (13)$$

In fact, this parameterization allows us to decouple the cost function $c^\theta(x, y)$ and the potential function $f^\theta(y)$. Specifically, changes in $f^\theta(y)$ can be offset by corresponding changes in $c^\theta(x, y)$, resulting in the same energy function $E^\theta(y|x)$. For example, by setting $f^\theta(y) \equiv 0$ and $\varepsilon = 1$, the parameterization of the energy function $E^\theta(y|x)$ remains consistent, as it can be exclusively derived from $c^\theta(x, y)$. By substituting (13) into the energy term in (12), we obtain:

$$\mathbb{E}_{x, y \sim \pi^*} E^\theta(y|x) = \frac{1}{\varepsilon} [\mathbb{E}_{x, y \sim \pi^*} [c^\theta(x, y)] - \mathbb{E}_{x, y \sim \pi^*} f^\theta(y)].$$

Note that the second term is independent of x . Thus, $\mathbb{E}_{x, y \sim \pi^*} f^\theta(y) = \mathbb{E}_{y \sim \pi_y^*} f^\theta(y)$. Finally, we obtain **our final objective** incorporating both paired and unpaired data:

$$\begin{aligned} \mathcal{L}(\theta) = & \underbrace{\varepsilon^{-1} \mathbb{E}_{x,y \sim \pi^*} [c^\theta(x,y)]}_{\text{Joint, requires pairs } (x,y) \sim \pi^*} \\ & - \underbrace{\varepsilon^{-1} \mathbb{E}_{y \sim \pi_y^*} f^\theta(y)}_{\text{Marginal, requires } x \sim \pi_x^*} + \underbrace{\mathbb{E}_{x \sim \pi_x^*} \log Z^\theta(x)}_{\text{Marginal, requires } x \sim \pi_x^*}. \end{aligned} \quad (14)$$

In Appendix D.1, we provide a rigorous sequence of equalities, starting from (5) and leading to (14). This derivation is carried out entirely through *formal mathematical transitions*. At this point, a reader may come up with 2 reasonable questions regarding (14):

1. How to perform the optimization of the proposed objective? This question is not straightforward due to the existence of the (typically intractable) normalizing constant Z_θ in the objective.
2. To which extent do the separate terms in (14) (paired, unpaired data) contribute to the objective, and which type of data is the most important to get the correct solution?

We answer these questions in §3.3 and §5. Before doing that, we show a surprising finding that our proposed objective exactly solves the inverse entropic OT problem (4).

3.2. Relation to Inverse Entropic Optimal Transport

In this section, we show that (4) is equivalent to (14). Indeed, substituting the dual form of entropic OT (2) into the inverse entropic OT problem with the omitted entropy yields (4):

$$\begin{aligned} \min_c \left[\mathbb{E}_{x,y \sim \pi^*} [c(x,y)] \right. \\ \left. - \max_f \left\{ \mathbb{E}_{x \sim \pi_x^*} f^c(x) + \mathbb{E}_{y \sim \pi_y^*} f(y) \right\} \right] = \quad (15) \\ \min_{c,f} \left\{ \mathbb{E}_{x,y \sim \pi^*} [c(x,y)] - \mathbb{E}_{x \sim \pi_x^*} f^c(x) - \mathbb{E}_{y \sim \pi_y^*} f(y) \right\}. \end{aligned}$$

Now, let's assume that both c and f are parameterized as c^θ and f^θ with respect to a parameter θ . Based on the definition provided in (3) and utilizing our energy function parameterization from (13), we can express $(f^\theta)^{c^\theta}(x)$ as:

$$(f^\theta)^{c^\theta}(x) = -\varepsilon \log Z^\theta(x). \quad (16)$$

This clarification shows that the expression in (15) aligns with our proposed likelihood-based loss in (14), scaled by ε . This finding indicates that *inverse entropic optimal transport (OT) can be interpreted as a likelihood maximization problem*, which opens up significant avenues to leverage established likelihood maximization techniques for optimizing inverse entropic OT, such as the evidence lower bound methods (Barber, 2012; Alemi et al., 2018) and expectation-maximization strategies (Bishop & Bishop, 2023), etc.

Moreover, this insight allows us to reframe inverse entropic OT as *addressing the semi-supervised domain translation problem*, as it facilitates the use of both paired data from π^*

and unpaired data from π_x^* and π_y^* . Notably, to our knowledge, the inverse OT problem has primarily been explored in *discrete* learning scenarios that assume access only to paired data (see the extended discussion in §4).

3.3. Practical Light Parameterization

The most computationally intensive aspect of optimizing the loss function in (14) lies in calculating the integral for the normalization constant Z^θ . To tackle this challenge, we propose a lightweight parameterization that yields closed-form expressions for each term in the loss function. Our proposed cost function parameterization c^θ is based on the log-sum-exp function (Murphy, 2012, §3.5.3):

$$c^\theta(x,y) = -\varepsilon \log \sum_{m=1}^M v_m^\theta(x) \exp\left(\frac{\langle a_m^\theta(x), y \rangle}{\varepsilon}\right), \quad (17)$$

where $\{v_m^\theta(x) : \mathbb{R}^{D_x} \rightarrow \mathbb{R}_+, a_m^\theta(x) : \mathbb{R}^{D_x} \rightarrow \mathbb{R}^{D_y}\}_{m=1}^M$ are arbitrary parametric functions, e.g., *neural networks*, with learnable parameters denoted by θ_c . This choice stems from an analysis of the proof provided in (Korotin et al., 2024), where we sought to identify a more general form of the function that could be effectively applied to our framework. Therefore, we likewise employ Gaussian mixture parametrization in the dual potential f^θ :

$$f^\theta(y) = \varepsilon \log \sum_{n=1}^N w_n^\theta \mathcal{N}(y | b_n^\theta, \varepsilon B_n^\theta), \quad (18)$$

where $\theta_f \stackrel{\text{def}}{=} \{w_n^\theta, b_n^\theta, B_n^\theta\}_{n=1}^N$ are learnable parameters of the potential, with $w_n^\theta \geq 0$, $b_n^\theta \in \mathbb{R}^{D_y}$, and $B_n^\theta \in \mathbb{R}^{D_y \times D_y}$ being a symmetric positive definite matrix. Thereby, our framework comprises a total of $\theta \stackrel{\text{def}}{=} \theta_f \cup \theta_c$ learnable parameters. For *clarity* and to *avoid notation overload*, we will omit the superscript $^\theta$ associated learnable parameters and functions in the subsequent formulas.

Proposition 3.1 (Tractable normalization constant). *Our parametrization of the cost function (17) and dual potential (18) delivers $Z^\theta(x) \stackrel{\text{def}}{=} \sum_{m=1}^M \sum_{n=1}^N z_{mn}(x)$, where*

$$z_{mn}(x) \stackrel{\text{def}}{=} w_n v_m(x) \exp\left(\frac{a_m^\top(x) B_n a_m(x) + 2b_n^\top a_m(x)}{2\varepsilon}\right).$$

The proposition offers a closed-form expression for $Z^\theta(x)$, which is essential for optimizing (14). Furthermore, our following proposition supplements the previous one and provides a method for sampling y given a new sample x_{new} .

Proposition 3.2 (Tractable conditional distributions). *From our parametrization of the cost function (17) and dual potential (18) it follows that the $\pi^\theta(\cdot|x)$ are Gaussian mixtures:*

$$\pi^\theta(y|x) = \frac{1}{Z^\theta(x)} \sum_{m=1}^M \sum_{n=1}^N z_{mn}(x) \mathcal{N}(y | d_{mn}(x), \varepsilon B_n), \quad (19)$$

where $d_{mn}(x) \stackrel{\text{def}}{=} b_n + B_n a_m(x)$.

TRAINING. Since we only have access to samples from the distributions (§2.1), we minimize the empirical counterpart of (14) via the stochastic gradient descent w.r.t. θ :

$$\begin{aligned} \mathcal{L}(\theta) \approx \widehat{\mathcal{L}}(\theta) \stackrel{\text{def}}{=} & \varepsilon^{-1} \frac{1}{P} \sum_{p=1}^P c^\theta(x_p, y_p) \\ & - \varepsilon^{-1} \frac{1}{R} \sum_{r=1}^R f^\theta(y_r) + \frac{1}{Q} \sum_{q=1}^Q \log Z^\theta(x_q). \end{aligned} \quad (20)$$

INFERENCE. According to our Proposition 3.2, the conditional distributions $\pi^\theta(\cdot|x)$ are Gaussian mixtures (19). As a result, sampling y given x is fast and straightforward.

3.4. Universal Approximation of the Light Parametrization

One may naturally wonder how expressive is our proposed parametrization of π_θ in §3.3. Below we show that this parametrization allows approximating **any** distribution π^* that satisfies mild compactness, boundness and regularity assumptions, see the [details](#) in Appendix D.4.

Theorem 3.3 (Light parametrization guarantees universal conditional distributions). *With mild assumptions on the joint distribution π^* , for all $\delta > 0$ there exists (a) an integer $N > 0$ and a Gaussian mixture f^θ (18) with N components, (b) an integer $M > 0$ and cost c^θ (17) defined by (b.1) fully-connected neural networks $a_m : \mathbb{R}^{D_x} \rightarrow \mathbb{R}^{D_y}$ with ReLU activations and (b.2) fully-connected neural networks $v_m : \mathbb{R}^{D_x} \rightarrow \mathbb{R}_+$ with ReLU activations such that π^θ defined by (11) and (13) satisfies $\text{KL}(\pi^* \|\pi^\theta) < \delta$.*

4. Related Works

We review below the most related semi-supervised models and OT-based approaches to our work.

Semi-supervised models. As discussed in §1, many existing semi-supervised domain translation methods combine paired and unpaired data by introducing multiple loss terms into *ad hoc optimization objectives*. Several works—such as (Jin et al., 2019, §3.3), (Tripathy et al., 2019, §3.5), (Oza et al., 2019, §C), (Paavilainen et al., 2021, §2), and (Panda et al., 2023, Eq. 8) — employ GAN-base objectives, which incorporate the GAN losses (Goodfellow et al., 2014) augmented with specific regularization terms to utilize paired data. Although most of these methods were initially designed for the image-to-image translation, their dependence on GAN objectives enables their application to broader domain translation tasks. In contrast, the approaches introduced by (Mustafa & Mantiuk, 2020, §3.2) and (Tang et al., 2024, Eq. 8) employ loss functions specifically tailored for the image-to-image translation, making them unsuitable for the general domain translation problem described in §2.1.

Another line of research explores methods based on *key-point guided OT* (Gu et al., 2022), which integrates paired

data information into the discrete transport plan. Building on this concept, (Gu et al., 2023) uses such transport plans as heuristics to train a conditional score-based model on unpaired or semi-paired data. Furthermore, the recent work (Theodoropoulos et al., 2024) speculatively incorporates paired data guidance directly into the cost function $c(x, y)$ of the standard formulation (1) and derives a dynamical formulation for this problem and a computational algorithm.

Importantly, the paradigms outlined above do not offer any theoretical guarantees for reconstructing the conditional distribution $\pi^*(y|x)$, as they depend on heuristic loss constructions. Furthermore, we show that such approaches actually fail to recover the true plan even in toy 2-dimensional cases, refer to experiments in §5 for an illustrative example.

We also note that there exist works addressing the question of incorporating unpaired data to the log-likelihood training (10) by adding an extra likelihood terms, see CNFs-related works (Atanov et al., 2019; Izmailov et al., 2020). However, they rely on x being a discrete object (e.g., a class label) and does not easily generalize to the continuous case, see Appendix C.2 for details.

(Inverse) OT solvers. As highlighted in §2.2, the task of inverse optimal transport (IOT) implies learning the cost function from samples drawn from an optimal coupling π^* . Existing IOT solvers (Dupuy et al., 2016; Li et al., 2019; Stuart & Wolfram, 2020; Galichon & Salanié, 2022) focus on reconstructing cost functions from discrete marginal distributions, in particular, using the log-likelihood maximization techniques (Dupuy et al., 2016), see the introduction of (Andrade et al., 2023) for a review. In contrast, we develop a log-likelihood based approach aimed at learning a conditional distribution $\pi^\theta(\cdot|x) \approx \pi^*(\cdot|x)$ that incorporates both paired and unpaired data but not the cost function itself.

Recent work by (Howard et al., 2024) proposes a framework for learning cost functions to improve the mapping between the domains. However, it is limited by the use of deterministic mappings, i.e., does not have the ability to model non-degenerate conditional distributions.

Another recent work by (Asadulaev et al., 2024) introduces a neural network-based OT framework for semi-supervised scenarios, utilizing general cost functionals for OT. However, their method requires **manually** constructing cost functions which can incorporate class labels or predefined pairs. In contrast, our method dynamically adjusts the cost function during training, offering a more flexible framework.

Our solver builds on the framework introduced by (Mokrov et al., 2024) and incorporates cost function optimization directly into the objective function, as outlined in equation (20), enabling effective handling of paired data. Additionally, we extend the light Gaussian Mixture parametrization proposed by (Korotin et al., 2024; Gushchin

et al., 2024), which was originally developed as a forward solver for entropic OT with a quadratic cost function $c^*(x, y) = \frac{1}{2}\|x - y\|_2^2$. Our work generalizes this solver to accommodate a wider variety of cost functions, as specified in equation (17). As a result, our approach also functions as a novel forward solver for these generalized cost functions.

5. Experimental Illustrations

We tested our solver on both synthetic data (§5.1) and real-world data distributions (§5.2). The code is written using the PyTorch framework and will be made publicly available. It is provided in the supplemental materials. Experimental details are given in Appendix B.

5.1. Gaussian To Swiss Roll Mapping

Setup. For illustration purposes, we adapt the setup described in (Mokrov et al., 2024; Korotin et al., 2024) for our needs and consider a synthetic task where we transform samples from a Gaussian distribution π_x^* into a Swiss Roll π_y^* distribution (Figure 2k). The plan π^* is generated by sampling from the mini-batch OT plan using the POT library (Flamary et al., 2021). We specifically choose a transportation cost (see Appendix C.1) for the mini-batch OT to construct a true plan π^* with bi-modal conditional distributions $\pi^*(\cdot|x)$ to assess how different methods are able to learn the multi-modal ground-truth. During training, we use $P = 128$ paired (Figure 2l) and $Q = R = 1024$ unpaired samples. We analyze the effect of varying the proportions of paired and unpaired data on our method’s performance in an ablation study detailed in Appendix C.4.

Baselines. We evaluate our method against:

1. **Semi-supervised log-likelihood** methods (Atanov et al., 2019; Izmailov et al., 2020): CNF (SS) and CGMM (SS).
2. **Semi-supervised methods:** Neural OT with pair-guided cost functional (Asadulaev et al., 2024, GNOT, Appendix E), differentiable cost-parameterized entropic mapping estimator (Howard et al., 2024, DCPHEME), (Panda et al., 2023, parOT), (Gu et al., 2023, OTCS).
3. **Standard generative & predictive models:** MLP regression with ℓ^2 loss, Unconditional GAN with ℓ^2 loss supplement (Goodfellow et al., 2014, UGAN+ ℓ^2), Conditional Generative Adversarial Network (Mirza & Osindero, 2014, CGAN), Conditional Normalizing Flow (Winkler et al., 2019, CNF).

For a detailed explanation of these baselines, see Appendix C.2. Note that some baselines can fully utilize both paired and unpaired data during training, while others rely solely on paired data. Refer to Table 3 for specifics on data usage.

Discussion. The results of the aforementioned methods are depicted in Figure 2. Clearly, the Regression model simply predicts the conditional mean $\mathbb{E}_{y \sim \pi^*(\cdot|x)} y$, failing to capture

the full distribution. The CGAN is unable to accurately learn the target distribution π_y^* , while the UGAN+ ℓ^2 fails to capture the underlying conditional distribution, resulting in suboptimal performance. The CNF model suffers from overfitting, likely due to the limited availability of paired data XY_{paired} . Methods GNOT, DCPHEME, parOT learn deterministic mapping and therefore unable to capture the conditional distribution. In turn, OTCS does not capture bi-modal conditional mapping. The CNF (SS) does not provide improvement compared to CNF in this experiment, and CGMM (SS) model learns a degenerate solution, which is presumably due to the overfitting. As a sanity check, we evaluate all baselines using a large amount of paired data. Details are given in Appendix C.3. In fact, even in this case, almost all the methods fail to learn true $\pi^*(\cdot|x)$.

5.2. Weather prediction

Here we aim to evaluate our proposed approach on real-world data. We consider the *weather prediction* dataset (Malinin et al., 2021; Rubachev et al., 2024). The data is collected from weather stations and weather forecast physical models. It consists of 94 meteorological features, e.g., pressure, wind, humidity, etc., which are measured over a period of one year at different spatial locations.

Setup. Initially, the problem was formulated as the prediction and uncertainty estimation of the air temperature at a specific time and location. We expand this task to the probabilistic prediction of all meteorological features, thereby reducing reliance on measurement equipment in remote and difficult-to-access locations, such as the Polar regions (see in Appendix B.3). We obtain 500 unpaired and 192 paired data samples. For testing, 100 pairs are randomly selected.

Metrics and baselines. We evaluate the performance of our approach by calculating the *log-likelihood* on the test target features. A natural baseline for this task is a probabilistic model that maximizes the likelihood of the target data. Thus, we implement an MLP that learns to predict the parameters of a mixture of Gaussians and is trained on the paired data only via the log-likelihood optimization (10). We also compare with semi-supervised log-likelihood methods CGMM (SS) and CNF (SS). For completeness, we also add standard generative models. These models are trained using the available paired and unpaired data. Note that GAN models do not provide the density estimation and log-likelihood can not be computed for them. Therefore, we include the conditional Freshet distance metric. Namely, for each test x we evaluate the Freshet distance (Heusel et al., 2017, Equation 6) between the predicted and the true features y . Then we average all these values obtained for all test inputs x .

Results. The results are presented in Tables 1 and 2. Result of Table 1 demonstrate that increasing the number of paired and unpaired data samples leads to improved test

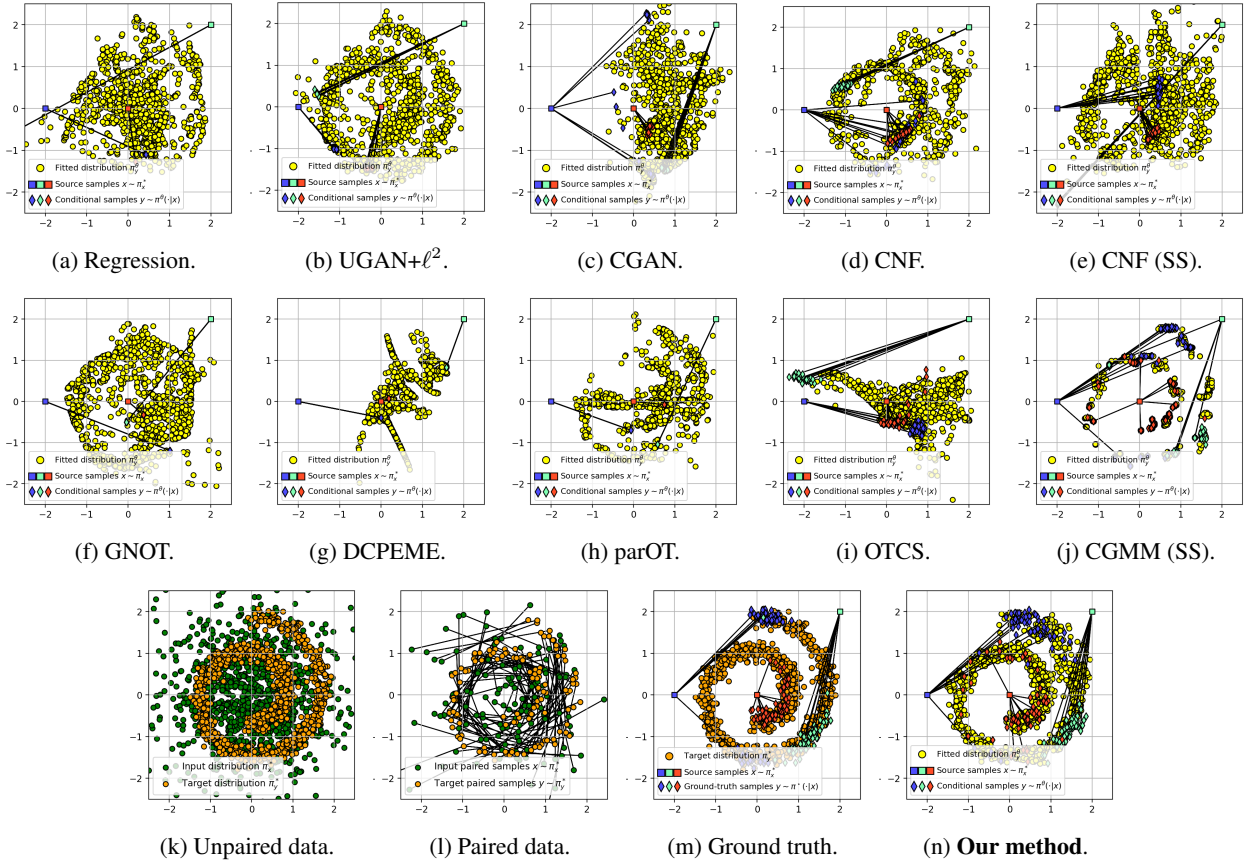


Figure 2. Comparison of the learned mapping on the *Gaussian* \rightarrow *Swiss Roll* task for $P = 128$ paired and $Q = R = 1024$ unpaired data.

# Paired	# Unpaired	Baseline		Ours				
		0	10	50	100	250	500	
10	0.4	17.9	18.5	18.4	18.8	19.2		
	$\pm .2$	$\pm .3$	$\pm .4$	$\pm .2$	$\pm .2$	$\pm .3$		
25	3.5	18.3	18.7	18.8	19.5	19.8		
	$\pm .09$	$\pm .06$	$\pm .2$	$\pm .07$	$\pm .1$	$\pm .1$		
50	6.4	18.7	18.9	19.2	19.8	20.3		
	$\pm .05$	$\pm .2$	$\pm .04$	$\pm .2$	$\pm .03$	$\pm .4$		
90	6.5	19	19.4	19.4	20.3	20.5		
	$\pm .1$	$\pm .01$	$\pm .05$	$\pm .2$	$\pm .05$	$\pm .09$		

Table 1. The values of the test *log-likelihood* \uparrow on the *weather prediction* dataset obtained for a different number of paired and unpaired training samples.

	Ours	CGAN	UGAN+l ²	CNF	Regression	CGMM (SS)	CNF (SS)
LL \uparrow	20.5 $\pm .09$	N/A	N/A	1.29 $\pm .03$	N/A	0.32 $\pm .03$	0.52 $\pm .02$
CFD \downarrow	7.21 $\pm .04$	15.79 ± 1.11	15.44 ± 1.89	18.72 $\pm .09$	8.29 $\pm .04$	7.17 $\pm .07$	28.5 $\pm .5$

Table 2. The values of the test *Log-Likelihood* (LL) and *Conditional Freshet distance* (CFD) on the *weather prediction* dataset of our approach and baselines (500 unpaired and 90 paired samples).

log-likelihood, which highlights the impact of the objective that employs both paired and unpaired data. Moreover, the proposed approach outperforms the baseline solution, which shows that even in problems where the paired data plays a key role for accurate predictions, incorporating the unpaired data can give an advantage. Additionally, the results in Ta-

ble 2 confirm that our approach produces samples closer to the true distributions compared to the other baselines (with 500 unpaired and 90 paired samples).

6. Discussion

Limitations. A limitation of our approach is its reliance on the Gaussian Mixture parameterization for modeling conditional distributions, which may hinder scalability. A promising direction for future research would be to explore more flexible parameterizations, such as neural networks. These have already been extensively studied in the context of forward entropic OT, as discussed in (Mokrov et al., 2024). For completeness, we provide an example in Appendix A demonstrating how fully neural parameterization can be applied to both the cost and potential functions for our loss via energy-based modeling (LeCun et al., 2006, EBM).

Potential impact. Our framework has a simple and non-minimax optimization objective that seamlessly incorporates both unpaired and paired samples into the training. We expect that these advantages will encourage the use of our framework to develop other max-likelihood-based semi-supervised approaches based on more advanced (than Gaussian mixtures) techniques, e.g., EBMs (Song & Kingma, 2021), diffusion models (Ho et al., 2020), etc.

Broader impact. This paper presents work whose goal is to advance the field of Machine Learning. There are many potential societal consequences of our work, none of which we feel must be specifically highlighted here.

References

- Acciaio, B., Kratsios, A., and Pammer, G. Designing universal causal deep learning models: The geometric (hyper) transformer. *Mathematical Finance*, 34(2):671–735, 2024.
- Agarap, A. F. Deep learning using rectified linear units (relu). *arXiv preprint arXiv:1803.08375*, 2018.
- Alemi, A., Poole, B., Fischer, I., Dillon, J., Saourous, R. A., and Murphy, K. Fixing a broken elbo. In *International conference on machine learning*, pp. 159–168. PMLR, 2018.
- Andrade, F., Peyré, G., and Poon, C. Sparsistency for inverse optimal transport. *arXiv preprint arXiv:2310.05461*, 2023.
- Andrieu, C., De Freitas, N., Doucet, A., and Jordan, M. I. An introduction to mcmc for machine learning. *Machine learning*, 50:5–43, 2003.
- Ansel, J., Yang, E., He, H., Gimelshein, N., Jain, A., Voznesensky, M., Bao, B., Bell, P., Berard, D., Burovski, E., Chauhan, G., Chourdia, A., Constable, W., Desmaison, A., DeVito, Z., Ellison, E., Feng, W., Gong, J., Gschwind, M., Hirsh, B., Huang, S., Kalambarkar, K., Kirsch, L., Lazos, M., Lezcano, M., Liang, Y., Liang, J., Lu, Y., Luk, C., Maher, B., Pan, Y., Puhersch, C., Reso, M., Saroufim, M., Siraichi, M. Y., Suk, H., Suo, M., Tillet, P., Wang, E., Wang, X., Wen, W., Zhang, S., Zhao, X., Zhou, K., Zou, R., Mathews, A., Chanan, G., Wu, P., and Chintala, S. Pytorch 2: Faster machine learning through dynamic python bytecode transformation and graph compilation. In *29th ACM International Conference on Architectural Support for Programming Languages and Operating Systems, Volume 2 (ASPLOS '24)*. ACM, April 2024. doi: 10.1145/3620665.3640366. URL <https://pytorch.org/assets/pytorch2-2.pdf>.
- Arabpour, R., Armstrong, J., Galimberti, L., Kratsios, A., and Livieri, G. Low-dimensional approximations of the conditional law of volta processes: a non-positive curvature approach. *arXiv preprint arXiv:2405.20094*, 2024.
- Arjovsky, M., Bottou, L., Gulrajani, I., and Lopez-Paz, D. Invariant risk minimization. *arXiv preprint arXiv:1907.02893*, 2019.
- Asadulaev, A., Korotin, A., Egiazarian, V., Mokrov, P., and Burnaev, E. Neural optimal transport with general cost functionals. In *The Twelfth International Conference on Learning Representations*, 2024.
- Atanov, A., Volokhova, A., Ashukha, A., Sosnovik, I., and Vetrov, D. Semi-conditional normalizing flows for semi-supervised learning. *arXiv preprint arXiv:1905.00505*, 2019.
- Backhoff-Veraguas, J. and Pammer, G. Applications of weak transport theory. *Bernoulli*, 28(1):370–394, 2022.
- Backhoff-Veraguas, J., Beiglböck, M., and Pammer, G. Existence, duality, and cyclical monotonicity for weak transport costs. *Calculus of Variations and Partial Differential Equations*, 58(6):203, 2019.
- Barber, D. *Bayesian reasoning and machine learning*. Cambridge University Press, 2012.
- Bishop, C. M. and Bishop, H. *Deep learning: Foundations and concepts*. Springer Nature, 2023.
- Carbone, D. Hitchhiker’s guide on energy-based models: a comprehensive review on the relation with other generative models, sampling and statistical physics. *arXiv preprint arXiv:2406.13661*, 2024.
- Carbone, D., Hua, M., Coste, S., and Vanden-Eijnden, E. Efficient training of energy-based models using jarzynski equality. *Advances in Neural Information Processing Systems*, 36:52583–52614, 2023.
- Cuturi, M. Sinkhorn distances: Lightspeed computation of optimal transport. *Advances in neural information processing systems*, 26, 2013.
- Cuturi, M., Klein, M., and Abblin, P. Monge, bregman and oc-cam: Interpretable optimal transport in high-dimensions with feature-sparse maps. In *International Conference on Machine Learning*, pp. 6671–6682. PMLR, 2023.
- Dinh, L., Sohl-Dickstein, J., and Bengio, S. Density estimation using real NVP. In *International Conference on Learning Representations*, 2017. URL <https://openreview.net/forum?id=HkpbH91x>.
- Du, Y., Li, S., Tenenbaum, B. J., and Mordatch, I. Improved contrastive divergence training of energy based models. In *Proceedings of the 38th International Conference on Machine Learning (ICML-21)*, 2021.
- Du, Y., Wang, W., Zhang, Z., Chen, B., Xu, T., Xie, J., and Chen, E. Non-parametric domain adaptation for end-to-end speech translation. In *Conference on Empirical Methods in Natural Language Processing (EMNLP)*, 2022.

- Dupuy, A., Galichon, A., and Sun, Y. Estimating matching affinity matrix under low-rank constraints. *arXiv preprint arXiv:1612.09585*, 2016.
- Flamary, R., Courty, N., Gramfort, A., Alaya, M. Z., Boissonunon, A., Chambon, S., Chapel, L., Corenflos, A., Fatras, K., Fournier, N., et al. Pot: Python optimal transport. *Journal of Machine Learning Research*, 22(78):1–8, 2021.
- Galichon, A. and Salanié, B. Cupid’s invisible hand: Social surplus and identification in matching models. *The Review of Economic Studies*, 89(5):2600–2629, 2022.
- Gao, R., Song, Y., Poole, B., Wu, Y. N., and Kingma, D. P. Learning energy-based models by diffusion recovery likelihood. In *International Conference on Learning Representations*, 2021.
- Genevay, A. *Entropy-regularized optimal transport for machine learning*. PhD thesis, Université Paris sciences et lettres, 2019.
- Geng, C., Han, T., Jiang, P.-T., Zhang, H., Chen, J., Hauberg, S., and Li, B. Improving adversarial energy-based model via diffusion process. In *Forty-first International Conference on Machine Learning*, 2024.
- Goodfellow, I., Pouget-Abadie, J., Mirza, M., Xu, B., Warde-Farley, D., Ozair, S., Courville, A., and Bengio, Y. Generative adversarial nets. *Advances in neural information processing systems*, 27, 2014.
- Gozlan, N., Roberto, C., Samson, P.-M., and Tetali, P. Kantorovich duality for general transport costs and applications. *Journal of Functional Analysis*, 273(11):3327–3405, 2017.
- Gu, X., Yang, Y., Zeng, W., Sun, J., and Xu, Z. Keypoint-guided optimal transport with applications in heterogeneous domain adaptation. *Advances in Neural Information Processing Systems*, 35:14972–14985, 2022.
- Gu, X., Yang, L., Sun, J., and Xu, Z. Optimal transport-guided conditional score-based diffusion model. *Advances in Neural Information Processing Systems*, 36:36540–36552, 2023.
- Gushchin, N., Kolesov, A., Mokrov, P., Karpikova, P., Spiridonov, A., Burnaev, E., and Korotin, A. Building the bridge of schrödinger: A continuous entropic optimal transport benchmark. *Advances in Neural Information Processing Systems*, 36:18932–18963, 2023.
- Gushchin, N., Kholkin, S., Burnaev, E., and Korotin, A. Light and optimal schrödinger bridge matching. In *Forty-first International Conference on Machine Learning*, 2024.
- Heusel, M., Ramsauer, H., Unterthiner, T., Nessler, B., and Hochreiter, S. Gans trained by a two time-scale update rule converge to a local nash equilibrium. *Advances in neural information processing systems*, 30, 2017.
- Ho, J., Jain, A., and Abbeel, P. Denoising diffusion probabilistic models. *Advances in neural information processing systems*, 33:6840–6851, 2020.
- Howard, S., Deligiannidis, G., Rebeschini, P., and Thornton, J. Differentiable cost-parameterized monge map estimators. *arXiv preprint arXiv:2406.08399*, 2024.
- Izmailov, P., Kirichenko, P., Finzi, M., and Wilson, A. G. Semi-supervised learning with normalizing flows. In *International conference on machine learning*, pp. 4615–4630. PMLR, 2020.
- Jiang, Q., Wang, M., Cao, J., Cheng, S., Huang, S., and Li, L. Learning kernel-smoothed machine translation with retrieved examples. In *Conference on Empirical Methods in Natural Language Processing (EMNLP)*, 2021.
- Jiang, Y., Jiang, L., Yang, S., and Loy, C. C. Scenimefy: Learning to craft anime scene via semi-supervised image-to-image translation. In *IEEE International Conference on Computer Vision (ICCV)*, 2023.
- Jin, C.-B., Kim, H., Liu, M., Jung, W., Joo, S., Park, E., Ahn, Y. S., Han, I. H., Lee, J. I., and Cui, X. Deep ct to mr synthesis using paired and unpaired data. *Sensors*, 19(10):2361, 2019.
- Joblove, G. H. and Greenberg, D. Color spaces for computer graphics. In *Proceedings of the 5th annual conference on Computer graphics and interactive techniques*, pp. 20–25, 1978.
- Kantorovich, L. V. On the translocation of masses. In *Dokl. Akad. Nauk. USSR (NS)*, volume 37, pp. 199–201, 1942.
- Kingma, D. P. Adam: A method for stochastic optimization. *arXiv preprint arXiv:1412.6980*, 2014.
- Korotin, A., Gushchin, N., and Burnaev, E. Light schrödinger bridge. In *The Twelfth International Conference on Learning Representations*, 2024.
- LeCun, Y., Chopra, S., Hadsell, R., Ranzato, M., Huang, F., et al. A tutorial on energy-based learning. *Predicting structured data*, 1(0), 2006.
- Li, R., Ye, X., Zhou, H., and Zha, H. Learning to match via inverse optimal transport. *Journal of machine learning research*, 20(80):1–37, 2019.
- Lin, J., Xia, Y., Qin, T., Chen, Z., and Liu, T.-Y. Conditional image-to-image translation. In *Computer Vision and Pattern Recognition (CVPR)*, 2018.

- Malinin, A., Band, N., Chesnokov, G., Gal, Y., Gales, M. J., Noskov, A., Ploskonosov, A., Prokhorenkova, L., Provilkov, I., Raina, V., et al. Shifts: A dataset of real distributional shift across multiple large-scale tasks. *arXiv preprint arXiv:2107.07455*, 2021.
- Mirza, M. and Osindero, S. Conditional generative adversarial nets. *CoRR*, abs/1411.1784, 2014. URL <http://arxiv.org/abs/1411.1784>.
- Mokrov, P., Korotin, A., Kolesov, A., Gushchin, N., and Burnaev, E. Energy-guided entropic neural optimal transport. In *The Twelfth International Conference on Learning Representations*, 2024.
- Moriakov, N., Adler, J., and Teuwen, J. Kernel of cycle-gan as a principal homogeneous space. In *International Conference on Learning Representations*, 2020.
- Morishita, M., Suzuki, J., and Nagata, M. Domain adaptation of machine translation with crowdworkers. In *Conference on Empirical Methods in Natural Language Processing (EMNLP)*, 2022.
- Murphy, K. P. *Machine learning: a probabilistic perspective*. MIT press, 2012.
- Mustafa, A. and Mantiuk, R. K. Transformation consistency regularization—a semi-supervised paradigm for image-to-image translation. In *Computer Vision—ECCV 2020: 16th European Conference, Glasgow, UK, August 23–28, 2020, Proceedings, Part XVIII 16*, pp. 599–615. Springer, 2020.
- Oza, M., Vaghela, H., and Bagul, S. Semi-supervised image-to-image translation. In *2019 International Conference of Artificial Intelligence and Information Technology (ICAIT)*, pp. 16–20. IEEE, 2019.
- Paavilainen, P., Akram, S. U., and Kannala, J. Bridging the gap between paired and unpaired medical image translation. In *MICCAI Workshop on Deep Generative Models*, pp. 35–44. Springer, 2021.
- Panda, N., Klein, N., Yang, D., Gasda, P., and Oyen, D. Semi-supervised learning of pushforwards for domain translation & adaptation. *arXiv preprint arXiv:2304.08673*, 2023.
- Papamakarios, G., Nalisnick, E., Rezende, D. J., Mohamed, S., and Lakshminarayanan, B. Normalizing flows for probabilistic modeling and inference. *Journal of Machine Learning Research*, 22(57):1–64, 2021.
- Peng, D., Hu, P., Ke, Q., and Liu, J. Diffusion-based image translation with label guidance for domain adaptive semantic segmentation. In *IEEE International Conference on Computer Vision (ICCV)*, 2023.
- Peyré, G., Cuturi, M., et al. Computational optimal transport: With applications to data science. *Foundations and Trends® in Machine Learning*, 11(5-6):355–607, 2019.
- Pinkus, A. Approximation theory of the mlp model in neural networks. *Acta numerica*, 8:143–195, 1999.
- Roberts, G. O. and Tweedie, R. L. Exponential convergence of langevin distributions and their discrete approximations. 1996.
- Ronneberger, O., Fischer, P., and Brox, T. U-net: Convolutional networks for biomedical image segmentation. In *Medical image computing and computer-assisted intervention—MICCAI 2015: 18th international conference, Munich, Germany, October 5-9, 2015, proceedings, part III 18*, pp. 234–241. Springer, 2015.
- Rubachev, I., Kartashev, N., Gorishniy, Y., and Babenko, A. Tabred: A benchmark of tabular machine learning in-the-wild. *arXiv preprint arXiv:2406.19380*, 2024.
- Santambrogio, F. Optimal transport for applied mathematicians. *Birkäuser, NY*, 55(58-63):94, 2015.
- Sason, I. On reverse pinsker inequalities. *arXiv preprint arXiv:1503.07118*, 2015.
- Song, Y. and Kingma, D. P. How to train your energy-based models. *arXiv preprint arXiv:2101.03288*, 2021.
- Stuart, A. M. and Wolfram, M.-T. Inverse optimal transport. *SIAM Journal on Applied Mathematics*, 80(1):599–619, 2020.
- Tang, X., Hu, X., Gu, X., and Sun, J. Residual-conditioned optimal transport: Towards structure-preserving unpaired and paired image restoration. In *Forty-first International Conference on Machine Learning*, 2024. URL <https://openreview.net/forum?id=irBHPlknxP>.
- Theodoropoulos, P., Komianos, N., Pacelli, V., Liu, G.-H., and Theodorou, E. A. Feedback schr {`" o} dinger bridge matching. *arXiv preprint arXiv:2410.14055*, 2024.
- Tripathy, S., Kannala, J., and Rahtu, E. Learning image-to-image translation using paired and unpaired training samples. In *Computer Vision—ACCV 2018: 14th Asian Conference on Computer Vision, Perth, Australia, December 2–6, 2018, Revised Selected Papers, Part II 14*, pp. 51–66. Springer, 2019.
- Vasluianu, F.-A., Romero, A., Van Gool, L., and Timofte, R. Shadow removal with paired and unpaired learning. In *Proceedings of the IEEE/CVF Conference on Computer Vision and Pattern Recognition*, pp. 826–835, 2021.
- Villani, C. et al. *Optimal transport: old and new*, volume 338. Springer, 2009.

- Winkler, C., Worrall, D. E., Hoogeboom, E., and Welling, M. Learning likelihoods with conditional normalizing flows. *CoRR*, abs/1912.00042, 2019. URL <http://arxiv.org/abs/1912.00042>.
- Yang, Z. and Chen, Z. Learning from paired and unpaired data: Alternately trained cyclegan for near infrared image colorization. In *2020 IEEE International Conference on Visual Communications and Image Processing (VCIP)*, pp. 467–470. IEEE, 2020.
- Yuan, Y., Liu, S., Zhang, J., Zhang, Y., Dong, C., and Lin, L. Unsupervised image super-resolution using cycle-in-cycle generative adversarial networks. In *Proceedings of the IEEE conference on computer vision and pattern recognition workshops*, pp. 701–710, 2018.
- Zhu, J.-Y., Park, T., Isola, P., and Efros, A. A. Unpaired image-to-image translation using cycle-consistent adversarial networks. In *Proceedings of the IEEE international conference on computer vision*, pp. 2223–2232, 2017.

A. Neural Parameterization

Throughout the main text, we parameterized the cost c^θ and potential f^θ using log-sum-exp functions and Gaussian mixtures (see §3.3). At this point, a reader may naturally wonder whether more general parameterizations for c^θ and f^θ can be used in our method, such as directly parameterizing both with neural networks. In this section, we affirmatively address this question by providing a procedure to optimize our main objective $\mathcal{L}(\theta)$ in (14) with general parameterizations for c^θ and f^θ .

A.1. Algorithm Derivation

We note that a key advantage of our chosen parameterization (see §3.3) is that the normalizing constant Z_θ appearing in $\mathcal{L}(\theta)$ is available in the closed form. Unfortunately, this is not the case with general parameterizations of c^θ and f^θ , necessitating the use of more advanced optimization techniques. While the objective $\mathcal{L}(\theta)$ itself may be intractable, we can derive its gradient, which is essential for optimization. The following proposition is derived in a manner similar to (Mokrov et al., 2024), who proposed methods for solving forward entropic OT problems with neural nets.

Proposition A.1 (Gradient of our main loss (14)). *It holds that*

$$\frac{\partial}{\partial \theta} \mathcal{L}(\theta) = \varepsilon^{-1} \left\{ \mathbb{E}_{x, y \sim \pi^*} \left[\frac{\partial}{\partial \theta} c^\theta(x, y) \right] - \mathbb{E}_{y \sim \pi_y^*} \left[\frac{\partial}{\partial \theta} f^\theta(y) \right] + \mathbb{E}_{x \sim \pi_x^*} \mathbb{E}_{y \sim \pi^\theta(y|x)} \left[\frac{\partial}{\partial \theta} (f^\theta(y) - c^\theta(x, y)) \right] \right\}.$$

The formula for the gradient no longer includes the intractable normalizing constant Z_θ . However, estimating the gradient requires sampling from the current model, i.e., obtaining $y \sim \pi^\theta(y|x)$. Unlike our Gaussian mixture-based parameterization (see §3.3), sampling from the model is more complex since we only have access to the unnormalized density of $\pi^\theta(y|x)$ through c^θ and f^θ , and it is not necessarily a Gaussian mixture in this case. Nevertheless, this sampling can be accomplished using techniques for sampling from unnormalized densities, such as Markov Chain Monte Carlo (MCMC) methods (Andrieu et al., 2003). Thus, the gradient of the loss can be practically estimated, leading us to the following gradient-based training Algorithm 1.

Algorithm 1: Semi-supervised Learning via Energy-Based Modeling

Input : Paired samples $XY_{\text{paired}} \sim \pi^*$; unpaired samples $X_{\text{unpaired}} \sim \pi_x^*$, $Y_{\text{unpaired}} \sim \pi_y^*$;
 potential network $f^\theta : \mathbb{R}^{D_y} \rightarrow \mathbb{R}$, cost network $c^\theta(x, y) : \mathbb{R}^{D_x} \times \mathbb{R}^{D_y} \rightarrow \mathbb{R}$;
 number of Langevin steps $K > 0$, Langevin discretization step size $\eta > 0$;
 basic noise std $\sigma_0 > 0$; batch sizes $\hat{P}, \hat{Q}, \hat{R} > 0$.

Output : trained potential network f^{θ^*} and cost network c^{θ^*} recovering $\pi^{\theta^*}(y|x)$ from (11).

for $i = 1, 2, \dots$ **do**

Derive batches $\{\hat{x}_p, \hat{y}_p\}_{p=1}^{\hat{P}} = XY \sim \pi^*$, $\{x_n\}_{n=1}^{\hat{Q}} = X \sim \pi_x^*$, $\{y_r\}_{r=1}^{\hat{R}} = Y \sim \pi_y^*$;
 Sample basic noise $Y^{(0)} \sim \mathcal{N}(0, \sigma_0)$ of size \hat{Q} ;
for $k = 1, 2, \dots, K$ **do**
 Sample $Z^{(k)} = \{z_q^{(k)}\}_{q=1}^{\hat{Q}}$, where $z_q^{(k)} \sim \mathcal{N}(0, 1)$;
 Obtain $Y^{(k)} = \{y_q^{(k)}\}_{q=1}^{\hat{Q}}$ with Langevin step:
 $y_q^{(k)} \leftarrow y_q^{(k-1)} + \frac{\eta}{2\varepsilon} \cdot \text{stop-grad} \left(\frac{\partial}{\partial y} [f^\theta(y) - c^\theta(x_q, y)] \Big|_{y=y_q^{(k-1)}} \right) + \sqrt{\eta} z_q^{(k)}$
 $\hat{\mathcal{L}} \leftarrow \frac{1}{\hat{P}} \left[\sum_{x_p, y_p \in XY} c^\theta(x_p, y_p) \right] + \frac{1}{\hat{Q}} \left[\sum_{y_q^{(K)} \in Y^{(K)}} f^\theta(y_q^{(K)}) \right] - \frac{1}{\hat{R}} \left[\sum_{y_r \in Y} f_\theta(y_r) \right]$;
 Perform a gradient step over θ by using $\frac{\partial \hat{\mathcal{L}}}{\partial \theta}$;

In the Algorithm 1, we employ the standard MCMC method called the Unadjusted Langevin Algorithm (ULA) (Roberts & Tweedie, 1996). For a detailed discussion on methods for training EBMs, refer to recent surveys (Song & Kingma, 2021; Carbone, 2024).

Overall, our proposed *inverse* OT algorithm turns to be closely related to the *forward* OT algorithm presented in (Mokrov et al., 2024, Algorithm 1). The key differences beside the obvious fact that algorithms solve different problems are **(1)** we learn the cost function c^θ during the training process; **(2)** our learning exploits both paired and unpaired samples.

Algorithms of this kind are usually called the **Energy-based models** (LeCun et al., 2006, EBM) because they parameterize the distributions of interest through their energy functions, i.e., minus logarithms of unnormalized densities. Specifically, in the case of Algorithm 1, we learn unnormalized densities $\pi^\theta(y|x) \propto \exp\left(\frac{f^\theta(y) - c^\theta(x,y)}{\varepsilon}\right)$ defined through their energy functions $\varepsilon^{-1}(c^\theta(x,y) - f^\theta(y))$. Below, we demonstrate a proof-of-concept performance of Algorithm 1 on two setups: an illustrative 2D example and colored images.

A.2. Illustrative Example

Setup. We begin with a 2D example to showcase the capability of Algorithm 1 to learn conditional plans using a fully neural network-based parametrization. Specifically, we conduct experiments on the *Gaussian* \rightarrow *Swiss Roll* mapping problem (see §5.1) using two datasets: one containing 128 paired samples (as described in §5.1) and another with 16K paired samples (detailed in Appendix C.3).

Discussion. It is worth noting that the model’s ability to fit the target distribution is influenced by the amount of labeled data used during training. When working with partially labeled samples (as shown in Figure 3a), the model’s fit to the target distribution is less accurate compared to using a larger dataset. However, even with limited labeled data, the model still maintains good accuracy in terms of the paired samples. On the other hand, when provided with fully labeled data (see Figure 3b), the model generates more consistent results and achieves a better approximation of the target distribution. A comparison of the results obtained using Algorithm 1 with neural network parametrization and those achieved using Gaussian parametrization (Figure 2n) reveals that Algorithm 1 exhibits greater instability. This observation aligns with the findings of (Mokrov et al., 2024, Section 2.2), which emphasize the instability and mode collapse issues commonly encountered when working with EBMs.

Implementation Details. We employ MLPs with hidden layer configurations of [128, 128] and [256, 256, 256], using *LeakyReLU*(0.2) for the parametrization of the potential f^θ and the cost c^θ , respectively. The learning rates are set to $lr_{\text{paired}} = 5 \times 10^{-4}$ and $lr_{\text{unpaired}} = 2 \times 10^{-4}$. The sampling parameters follow those specified in (Mokrov et al., 2024).

A.3. Colored Images Example

Setup. We adapted an experiment from (Mokrov et al., 2024) using the colored MNIST dataset (Arjovsky et al., 2019). While the original task involved translating digit 2 into digit 3 using unpaired images, we modified the setup to demonstrate our method’s ability to perform translations according to paired data. Namely, we created pairs by shifting the hue (Joblove & Greenberg, 1978) of the source images by 120° . Specifically, for a source image with a hue h in the range $0^\circ \leq h < 360^\circ$, the target image’s hue was set to $(h + 120^\circ) \bmod 360^\circ$.

Discussion. The results of this experiment are shown in Figure 4. Notably, our method successfully learned the color transformation using only 10 pairs (third row). Increasing the number of pairs to 200 further improved the quality of the translation (forth row).

Implementation Details. We adopt the same parameters as in (Mokrov et al., 2024), with the exception of the cost function:

$$c^\theta(x, y) = \frac{1}{D_y} \|U_{\text{net}}^\theta - y\|_2^2.$$

Here, the dimensions of source and target spaces are $D_x = D_y = 3 \times 32 \times 32$ and $U_{\text{net}}^\theta : \mathbb{R}^{D_x} \rightarrow \mathbb{R}^{D_y}$ is a neural net function with U-Net architecture (Ronneberger et al., 2015) with 16 layers. The first layer has 64 filters, and the number of filters doubles in each subsequent layer.

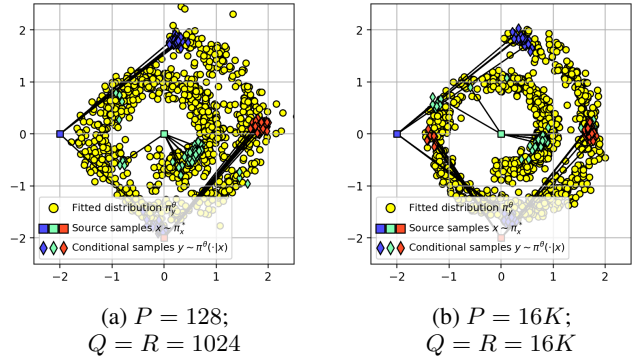


Figure 3. Performance of our Algorithm 1 in the *Gaussian* \rightarrow *Swiss Roll* mapping task (§5.1). We use MLPs to parametrize both the potential function f^θ and the cost function c^θ .

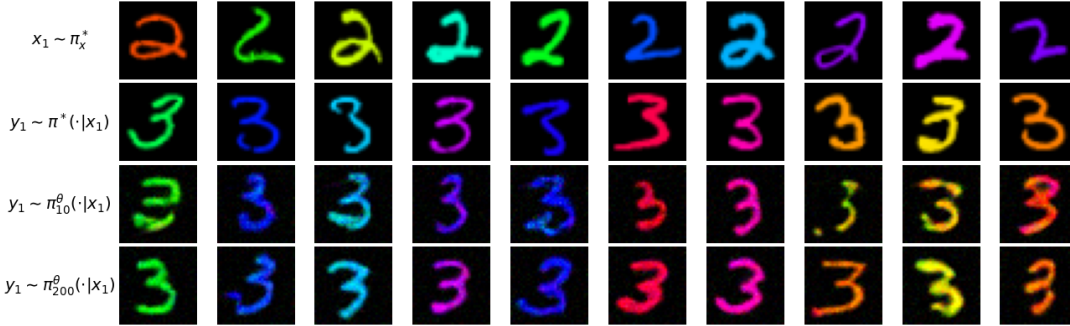


Figure 4. Performance of our Algorithm 1 on the colored MNIST mapping task. Each pair consists of digits 2 and 3 with a hue shift of 120° . The first row shows the source images, the second row displays target images with ground-truth colors, the third row presents the mapping results for 10 pairs in the train data, and the fourth row shows results for 200 pairs.

A.4. Conclusion

It is important to recognize that the field of Energy-Based Models has undergone significant advancements in recent years, with the development of numerous scalable approaches. For examples of such progress, we refer readers to recent works by (Geng et al., 2024; Carbone et al., 2023; Du et al., 2021; Gao et al., 2021) and other the references therein. Additionally, we recommend the comprehensive tutorial by (Song & Kingma, 2021; Carbone, 2024) for an overview of training methods for EBMs. Given these advancements, it is reasonable to expect that by incorporating more sophisticated techniques into our basic Algorithm 1, it may be possible to scale the method to handle high-dimensional setups, such as image data. However, exploring these scaling techniques is beyond the scope of the current paper, which primarily focuses on the general methodology for semi-supervised domain translation. The investigation of methods to further scale our approach as a promising future research avenue.

B. General Details of Experiments

B.1. General Implementation Details

Parametrization. The depth and number of hidden layers vary depending on the experiment.

For f^θ (18) we represent:

- w_n as $\log w_n$,
- b_n directly as a vector,
- the matrix B_n in diagonal form, with $\log(B_n)_{i,i}$ on its diagonal. This choice not only reduces the number of learnable parameters in θ_f but also enables efficient computation of B_n^{-1} with a time complexity of $\mathcal{O}(D_y)$.

For c^θ (17), we represent:

- $v_m(x)$ as a multilayer perceptron (MLP) with ReLU activations (Agarap, 2018) and a LogSoftMax output layer,
- $a_m(x)$ as an MLP with ReLU activations.

Optimizers. We employ two separate Adam optimizers (Kingma, 2014) with different step sizes for paired and unpaired data to enhance convergence.

Initialization.

- $\log w_n$ as $\log \frac{1}{n}$,
- b_n using random samples from π_y^* ,
- $\log(B_n)_{j,j}$ with $\log(0.1)$,
- for the neural networks, we use the default PyTorch initialization (Ansel et al., 2024),
- $\varepsilon = 1$ for all experiments, since the solver is independent of ε , as discussed in §2.2.

B.2. Gaussian To Swiss Roll Mapping

Implementation Details. We choose the parameters as follows: $N = 50, M = 25$, with learning rates $lr_{\text{paired}} = 3 \times 10^{-4}$ and $lr_{\text{unpaired}} = 0.001$. We utilize a two-layer MLP network for the function $a_m(x)$ and a single-layer MLP for $v_m(x)$. The experiments are executed in parallel on a 2080 Ti GPU for a total of 25,000 iterations, taking approximately 20 minutes to complete.

B.3. Weather prediction

We select two distinct months from the dataset and translate the meteorological features from the source month (January) to the target month (June). To operate at the monthly scale, we represent a source data point $x \in \mathbb{R}^{188}$ as the mean and standard deviation of the features collected at a specific location over the source month. The targets $y \in \mathbb{R}^{94}$ correspond to individual measurements in the target month. Pairs are constructed by aligning a source data point with the target measurements at the same location. Consequently, multiple target data points y may correspond to a single source point x and represent samples from conditional distributions $\pi^*(y|x)$. The measurements from non-aligned locations are treated as unpaired.

Implementation details. In general, we consider the same setting as in B.2. Specifically, we set $N = 10, M = 1$ and the number of optimization steps to 30,000. The baseline uses an MLP network with the same number of parameters, predicting the parameters of a mixture of 10 Gaussians.

C. Gaussian To Swiss Roll Mapping

C.1. Transportation cost matrix

To create the ground truth plan π^* , we utilize the following procedure: sample a mini-batch of size 64 and then determine the optimal mapping using the entropic Sinkhorn algorithm, as outlined in (Cuturi, 2013) and implemented in (Flamary et al., 2021). This process is repeated P times to generate the required number of pairs.

We define the cost matrix for mini-batch OT as $C = \min(C^{+\varphi}, C^{-\varphi})$, where $C^{\pm\varphi}$ represents matrices of pairwise ℓ_2 distances between x and $-y^{\pm\varphi}$, with $-y^{\pm\varphi}$ denoting the vector $-y$ rotated by an angle of $\varphi = \pm 90^\circ$. In other words, $x \sim \pi_x^*$ maps to y located on the opposite side of the Swiss Roll, rotated by either φ or $-\varphi$, as shown in Figure 2m.

C.2. Baseline Details

This section details the loss functions employed by the baseline models, providing context and explanation for the data usage summarized in Table 3. Furthermore, it explains a straightforward adaptation of the log-likelihood loss function presented in (10) to accommodate unpaired data, offering a natural comparative approach to the method proposed in our work. Finally, it includes details about our reproduction of other methods.

1. Standard generative & predictive models:

- **Regression Model** (MLP) uses the following simple ℓ^2 loss

$$\min_{\theta} \mathbb{E}_{(x,y) \sim \pi^*} \|y - G_{\theta}(x)\|^2,$$

where $G_{\theta} : \mathcal{X} \rightarrow \mathcal{Y}$ is a generator MLP with trainable parameters θ . Clearly, such a model can use only paired data. Furthermore, it is known that the optimal regressor G^* coincides with $\mathbb{E}_{y \sim \pi^*(\cdot|x)} y$, i.e., predicts the conditional expectation. Therefore, such a model will never learn the true data distribution unless all $\pi^*(\cdot|x)$ are degenerate.

Method	Paired $(x, y) \sim \pi^*$	Unpaired $x \sim \pi_x^*$	Unpaired $y \sim \pi_y^*$
Regression	✓	✗	✗
UGAN + ℓ^2	✓	✓	✓
CGAN	✓	✓	✗
CNF	✓	✗	✗
CNF (SS)	✓	✓	✓
GNOT	✓	✓	✓
DCPEME	✓	✓	✓
parOT	✓	✓	✓
OTCS	✓	✓	✓
CGMM (SS)	✓	✓	✓
Our method	✓	✓	✓

Table 3. The ability to use paired/unpaired data by various models.

- **Conditional GAN** uses the following min max loss:

$$\min_{\theta} \max_{\phi} \left[\underbrace{\mathbb{E}_{x,y \sim \pi^*} \log(D_{\phi}(y|x))}_{\text{Joint, requires pairs } (x,y) \sim \pi^*} + \underbrace{\mathbb{E}_{x \sim \pi_x^*} \mathbb{E}_{z \sim p_z} \log(1 - D_{\phi}(G_{\theta}(z|x)))}_{\text{Marginal, requires } x \sim \pi_x^*} \right],$$

where $G_{\theta} : \mathcal{Z} \times \mathcal{X} \rightarrow \mathcal{Y}$ is the conditional generator with parameters θ , p_z is a distribution on latent space \mathcal{Z} , and $D : \mathcal{Y} \times \mathcal{X} \rightarrow (0, 1)$ is the conditional discriminator with parameters ϕ . From the loss it is clear that the model can use not only paired data during the training, but also samples from π_x^* . The minimum of this loss is achieved when $G(\cdot|x)$ generates $\pi^*(\cdot|x)$ from p_z .

- **Unconditional GAN + ℓ^2 loss** optimizes the following min max objective:

$$\min_{\theta} \max_{\phi} \left[\lambda \underbrace{\mathbb{E}_{(x,y) \sim \pi^*} \mathbb{E}_{z \sim p_z} \|y - G_{\theta}(x,z)\|^2}_{\text{Joint, requires pairs } (x,y) \sim \pi^*} + \underbrace{\mathbb{E}_{y \sim \pi_y^*} \log(D_{\phi}(y))}_{\text{Marginal, requires } y \sim \pi_y^*} + \underbrace{\mathbb{E}_{x \sim \pi_x^*} \mathbb{E}_{z \sim p_z} \log(1 - D_{\phi}(G_{\theta}(x,z)))}_{\text{Marginal, requires } x \sim \pi_x^*} \right],$$

where $\lambda > 0$ is a hyperparameter. In turn, $G_{\theta} : \mathcal{X} \times \mathcal{Z} \rightarrow \mathcal{Y}$ is the stochastic generator. Compared to the unconditional case, the main idea here is to use the unconditional discriminator $D_{\phi} : \mathcal{Y} \rightarrow (0, 1)$. This allows using unpaired samples from π_y^* . However, using only GAN loss would not allow to use the paired information in any form, this is why the supervised ℓ^2 loss is added ($\lambda = 1$).

We note that this model has a trade-off between the target matching loss (GAN loss) and regression loss (which suffers from averaging). Hence, the model is unlikely to learn the true paired data distribution and can be considered a heuristical loss to use both paired and unpaired data. Overall, we consider this baseline as most existing GAN-based solutions (Tripathy et al., 2019, §3.5), (Jin et al., 2019, §3.3), (Yang & Chen, 2020, §C), (Vasluianu et al., 2021, §3) for paired and unpaired data use objectives that are *ideologically* similar to this one.

- **Conditional Normalizing Flow** (Winkler et al., 2019) learns an explicit density model

$$\pi^{\theta}(y|x) = p_z(G_{\theta}^{-1}(y|x)) \left| \frac{\partial G_{\theta}^{-1}(y|x)}{\partial y} \right|$$

via optimizing log-likelihood (10) of the paired data. Here $G_{\theta} : \mathcal{Z} \times \mathcal{X} \rightarrow \mathcal{Y}$ is the conditional generator function. It is assumed that $\mathcal{Z} = \mathcal{Y}$ and $G_{\theta}(\cdot|x)$ is invertible and differentiable. In the implementation, we use the well-celebrated RealNVP neural architecture (Dinh et al., 2017). The optimal values are attached when the generator $G_{\theta}(\cdot|x)$ indeed generates $\pi^{\theta}(\cdot|x) = \pi^*(\cdot|x)$.

The conditional flow is expected to accurately capture the true conditional distributions, provided that the neural architecture is sufficiently expressive and there is an adequate amount of paired data available. However, as mentioned in §3.1, a significant challenge arises in integrating unpaired data into the learning process. For instance, approaches such as those proposed by (Atanov et al., 2019; Izmailov et al., 2020) aim to extend normalizing flows to a semi-supervised context. However, these methods primarily assume that the input conditions x are discrete, making it difficult to directly apply their frameworks to our continuous case. For completeness, below we discuss a variant of the log-likelihood loss (Atanov et al., 2019, Eq. 1) when both x, y are continuous.

2. Semi-supervised log-likelihood methods (Atanov et al., 2019; Izmailov et al., 2020):

- **Semi-supervised Conditional Normalizing Flows.** As noted by the the authors, a natural strategy for log-likelihood semi-supervised training that leverages both paired and unpaired data is to optimize the following loss:

$$\max_{\theta} \left[\underbrace{\mathbb{E}_{(x,y) \sim \pi^*} \log \pi^{\theta}(y|x)}_{\text{Joint, requires pairs } (x,y) \sim \pi^*} + \underbrace{\mathbb{E}_{y \sim \pi_y^*} \log \pi^{\theta}(y)}_{\text{Marginal, requires } y \sim \pi_y^*} \right]. \quad (21)$$

This straightforward approach involves adding the unpaired data component, $\mathbb{E}_{y \sim \pi_y^*} \log \pi^{\theta}(y)$ to the loss function alongside the standard paired data component (10). While loss (21) looks natural, its optimization is **highly non-trivial** since the marginal log-likelihood $\log \pi^{\theta}(y)$ is not directly available. In fact, (Atanov et al., 2019; Izmailov et al., 2020) use this loss *exclusively* in the case when x is a discrete object, e.g., the class label $x \in \{1, 2, \dots, K\}$. In this case $\log \pi^{\theta}(y)$ can be analytically computed as the following finite sum

$$\log \pi^{\theta}(y) = \log \mathbb{E}_{x \sim \pi_x^*} \pi^{\theta}(y|x) = \log \sum_{k=1}^K \pi^{\theta}(y|x=k) \pi_x^*(x=k),$$

and $\pi^*(x = k)$ are known class probabilities. Unfortunately, in the continuous case $\pi_x^*(x)$ is typically not available explicitly, and one has to exploit **approximations** such as

$$\log \pi^\theta(y) = \log \mathbb{E}_{x \sim \pi_x^*} \pi^\theta(y|x) \approx \log \frac{1}{Q} \sum_{q=1}^Q \log \pi^\theta(y|x_q),$$

where x_q are train (unpaired) samples. However, such Monte-Carlo estimates are generally **biased** (because of the logarithm) and do not lead to good results, especially in high dimensions. Nevertheless, for completeness, we also test how this approach performs. In our 2D example (Figure 2e), we found there is no significant difference between this loss and the fully supervised loss (10): both models incorrectly map to the target and fail to learn conditional distributions.

- **Semi-supervised Conditional Gaussian Mixture Model.** Using above-discussed natural loss (21) for semi-supervised learning, one may also consider a (conditional) Gaussian mixture parametrization for $\pi^\theta(y|x)$ instead of the conditional normalizing flow. For completeness of the exposition, we also include such a baseline for comparison. For better transparency and fair comparison, we use the same Gaussian mixture parametrization (19) as in our method. We found that such a loss quickly overfits to data and leads to degenerate solutions, see Figure 2j.

3. **Semi-supervised Methods.** These methods are designed to learn deterministic OT maps with general cost functions and, as a result, cannot capture stochastic conditional distributions.

- **Neural optimal transport with pair-guided cost functional** (Asadulaev et al., 2024, GNOT). This method implies a general cost function for the neural optimal transport approach. A neural parametrization for the mapping function and potentials was used. In our experiments, we considered the settings of the paired cost function, which allows to utilize both paired and unpaired data. We used the publicly available implementation¹, which was verified for the toy experiments provided in the repository.
- **Differentiable cost-parameterized entropic mapping estimator** (Howard et al., 2024, DCPEME). We obtained the implementation from the authors but were unable to achieve satisfactory performance. This is likely due to the deterministic map produced by their method based on the entropic map estimator from (Cuturi et al., 2023). In particular, scenarios where nearby or identical points are mapped to distant locations may introduce difficulties, potentially leading to optimization stagnation during training.
- **Parametric Pushforward Estimation With Map Constraints** (Panda et al., 2023, parOT)². We evaluated this method using the ℓ_2 cost function, where it performed as expected. However, on our setup the method occurred unsuitable because it learns a fully deterministic transport map, which lacks the flexibility needed to model stochastic multimodal mapping. This limitation is visually evident in Figure 5h.
- **Optimal Transport-guided Conditional Score-based diffusion model.** (Gu et al., 2023, OTCS). We evaluated this method on a two-dimensional example from their GitHub repository³, where it performed as expected. However, when applied to our setup (described in §5.1), the method failed to yield satisfactory results, even when provided with a large amount of training data (refer to Figure 5i and detailed in Appendix C.3).

C.3. Baselines for Swiss Roll with the Large Amount of Data (16k)

In this section, we show the results of training of the baselines on the large amount of both paired (16K) and unpaired (16K) data (Figure 5). Recall that the ground truth π^* is depicted in Figure 2m.

As expected, Regression fails to learn anything meaningful due to the averaging effect (Figure 5a). In contrast, the unconditional GAN+ ℓ^2 (Figure 5b) nearly succeeds in generating the target data π_y^* , but the learned plan is incorrect because of the averaging effect. Given a sufficient amount of training data, **Conditional GAN** (Figure 5c) nearly succeeds in learning the true conditional distributions $\pi^*(\cdot|x)$. The same applies to the conditional normalizing flow (Figure 5d), but its results are slightly worse, presumably due to the limited expressiveness of invertible flow architecture.

Experiments using the natural semi-supervised loss function in (21) demonstrate that this loss function can reasonably recover the conditional mapping with both CNF (Figure 5e) and CGMM (Figure 5j) parameterizations. However, it requires

¹<https://github.com/machinestein/GNOT>

²<https://github.com/natalieklein229/uq4ml/tree/parot>

³<https://github.com/XJTU-XGU/OTCS/>

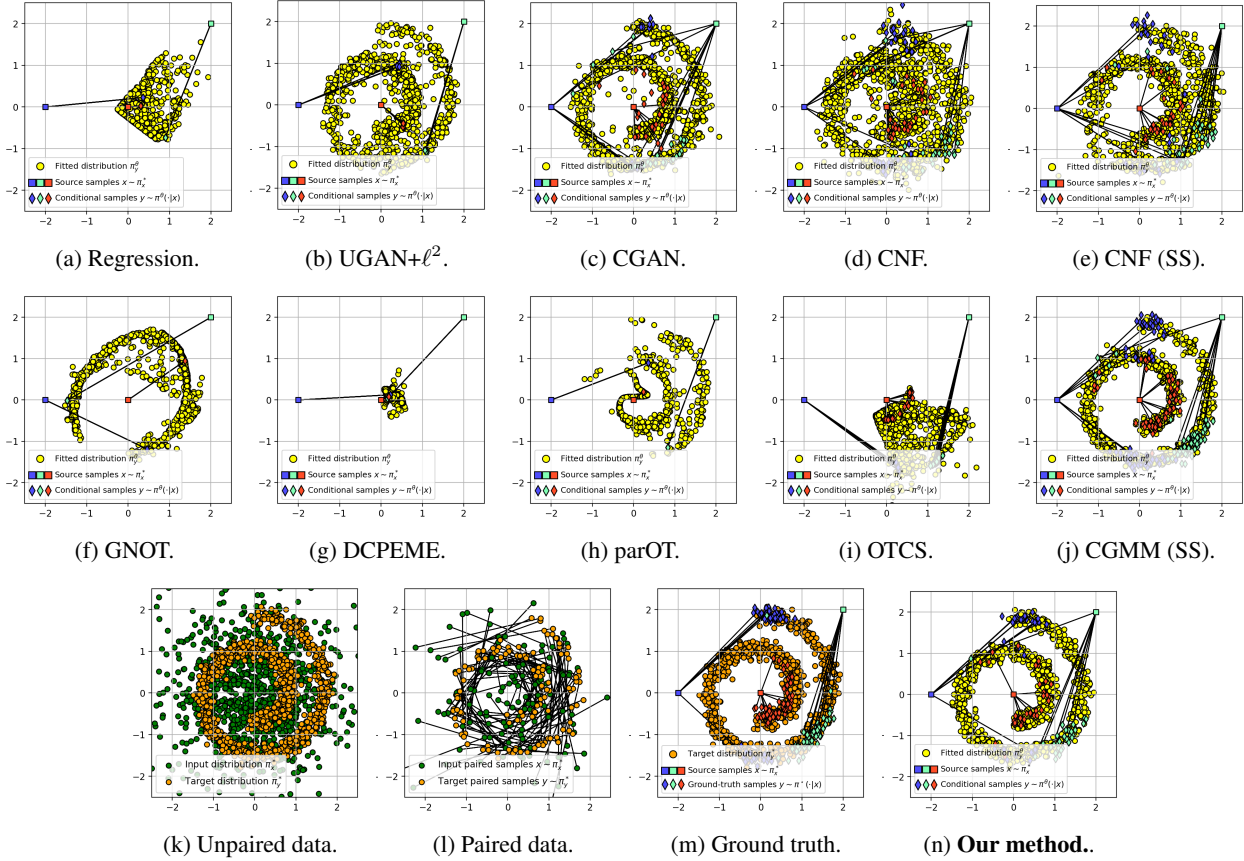


Figure 5. Comparison of the mapping learned by baselines on *Gaussian* \rightarrow *Swiss Roll* task (§5.1). We use $P = 16K$ paired data, $Q = R = 16K$ unpaired data for training.

significantly more training data compared to our proposed loss function (14). This conclusion is supported by the observation that the CGMM model trained with (21) tends to overfit, as shown in Figure 2j. In contrast, our method, which uses the objective (14), achieves strong results, as illustrated in Figure 2n.

Other methods, unfortunately, also struggle to handle this toy illustrative 2D task effectively, despite their success in large-scale problems. This discrepancy raises questions about the theoretical justification and general applicability of these methods, particularly in scenarios where simpler tasks reveal limitations not evident in more complex settings.

C.4. Ablation study

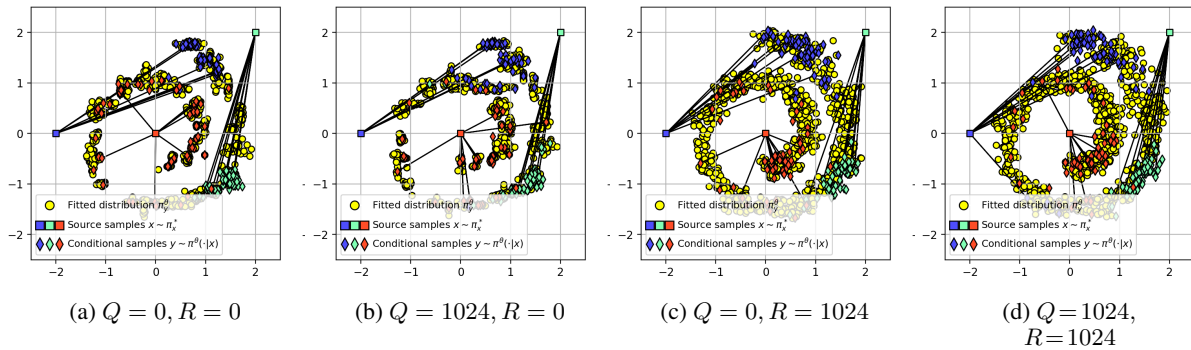


Figure 6. Ablation study analyzing the impact of varying source and target data point quantities on the learned mapping for the *Gaussian* \rightarrow *Swiss Roll* task (using $P = 128$ paired samples).

In this section, we conduct an ablation study to address the question posed in §3.1 regarding how the number of source and target samples influences the quality of the learned mapping. The results, shown in Figure 6, indicate that the quantity of target points R has a greater impact than the number of source points Q (compare Figure 6c with Figure 6b). Additionally, it is evident that the inclusion of unpaired data helps mitigate over-fitting, as demonstrated in Figure 6a.

D. Proofs

D.1. Loss Derivation

Below, we present a step-by-step derivation of the mathematical transitions, allowing the reader to follow and verify the validity of our approach. We denote as C_1, C_2 all terms that are not involved in learning the conditional plan $\pi^\theta(y|x)$, i.e., not dependent on θ . Starting from (5), we deduce

$$\begin{aligned}
 \text{KL}(\pi^* \|\pi^\theta) &= \mathbb{E}_{x,y \sim \pi^*} \log \frac{\pi_x^*(x)\pi^*(y|x)}{\pi_x^\theta(x)\pi^\theta(y|x)} = \mathbb{E}_{x \sim \pi_x^*} \log \frac{\pi_x^*(x)}{\pi_x^\theta(x)} + \mathbb{E}_{x,y \sim \pi^*} \log \frac{\pi^*(y|x)}{\pi^\theta(y|x)} = \\
 \text{KL}(\pi_x^* \|\pi_x^\theta) + \mathbb{E}_{x \sim \pi_x^*} \mathbb{E}_{y \sim \pi^*(\cdot|x)} \log \frac{\pi^*(y|x)}{\pi^\theta(y|x)} &= \underbrace{\text{KL}(\pi_x^* \|\pi_x^\theta)}_{\text{Marginal}} + \underbrace{\mathbb{E}_{x \sim \pi_x^*} \text{KL}(\pi^*(\cdot|x) \|\pi^\theta(\cdot|x))}_{\text{Conditional}} = \\
 C_1 + \mathbb{E}_{x \sim \pi_x^*} \mathbb{E}_{y \sim \pi^*(\cdot|x)} \log \frac{\pi^*(y|x)}{\pi^\theta(y|x)} &= C + \mathbb{E}_{x \sim \pi_x^*} \mathbb{E}_{y \sim \pi^*(\cdot|x)} [\log \pi^*(y|x) - \log \pi^\theta(y|x)] = \\
 C_1 - \mathbb{E}_{x \sim \pi_x^*} \text{H}(\pi^*(\cdot|x)) - \mathbb{E}_{x,y \sim \pi^*} \log \pi^\theta(y|x) &= C_2 - \mathbb{E}_{x,y \sim \pi^*} \log \pi^\theta(y|x) = \\
 C_2 - \mathbb{E}_{x,y \sim \pi^*} \log \frac{\exp(-E^\theta(y|x))}{Z^\theta(x)} &= C_2 + \mathbb{E}_{x,y \sim \pi^*} E^\theta(y|x) + \mathbb{E}_{x,y \sim \pi^*} \log Z^\theta(x) = \\
 C_2 + \mathbb{E}_{x,y \sim \pi^*} \frac{c^\theta(x,y) - f^\theta(y)}{\varepsilon} + \mathbb{E}_{x,y \sim \pi^*} \log Z^\theta(x) &= \\
 C_2 + \varepsilon^{-1} \mathbb{E}_{x,y \sim \pi^*} [c^\theta(x,y)] - \varepsilon^{-1} \mathbb{E}_{x,y \sim \pi^*} f^\theta(y) + \mathbb{E}_{x,y \sim \pi^*} \log Z^\theta(x) &= \\
 C_2 + \varepsilon^{-1} \mathbb{E}_{x,y \sim \pi^*} [c^\theta(x,y)] - \varepsilon^{-1} \mathbb{E}_{y \sim \pi_y^*} \mathbb{E}_{x \sim \pi^*(\cdot|y)} f^\theta(y) + \mathbb{E}_{x \sim \pi_x^*} \mathbb{E}_{y \sim \pi^*(\cdot|x)} \log Z^\theta(x) &= \\
 C_2 + \varepsilon^{-1} \mathbb{E}_{x,y \sim \pi^*} [c^\theta(x,y)] - \varepsilon^{-1} \mathbb{E}_{y \sim \pi_y^*} f^\theta(y) \underbrace{\mathbb{E}_{x \sim \pi^*(\cdot|y)} 1}_{=1} + \mathbb{E}_{x \sim \pi_x^*} \log Z^\theta(x) \underbrace{\mathbb{E}_{y \sim \pi^*(\cdot|x)} 1}_{=1} &= \\
 C_2 + \varepsilon^{-1} \mathbb{E}_{x,y \sim \pi^*} [c^\theta(x,y)] - \varepsilon^{-1} \mathbb{E}_{y \sim \pi_y^*} f^\theta(y) + \mathbb{E}_{x \sim \pi_x^*} \log Z^\theta(x). &
 \end{aligned}$$

The mathematical derivation presented above demonstrates that our defined loss function (14) is essentially a framework for minimizing KL-divergence. In other words, when the loss (14) equals to $-C_2$, it implies that we have successfully recovered the true conditional plan π^* in the KL sense.

D.2. Expressions for the Gaussian Parametrization

Proof of Proposition 3.1. Thanks to our parametrization of the cost c^θ (17) and the dual potential f^θ (18), we obtain:

$$\begin{aligned}
 \exp\left(\frac{f^\theta(y) - c^\theta(x,y)}{\varepsilon}\right) &= \exp\left(\log \sum_{n=1}^N w_n \mathcal{N}(y | b_n, \varepsilon B_n) + \log \sum_{m=1}^M v_m(x) \exp\left(\frac{\langle a_m(x), y \rangle}{\varepsilon}\right)\right) \\
 &= \sum_{m=1}^M \sum_{n=1}^N \frac{v_m(x) w_n}{\sqrt{\det(2\pi B_n^{-1})}} \exp\left(-\frac{1}{2}(y - b_n)^\top \frac{B_n^{-1}}{\varepsilon} (y - b_n) + \frac{\langle a_m(x), y \rangle}{\varepsilon}\right)
 \end{aligned}$$

Now we need to transform the expression above into the form of a Gaussian Mixture Model. To achieve this, we rewrite the formula inside the exponent using the fact that B_n is a symmetric:

$$\begin{aligned}
 (y - b_n)^\top B_n^{-1} (y - b_n) - 2\langle a_m(x), y \rangle &= y^\top B_n^{-1} y - 2b_n^\top B_n^{-1} y + b_n^\top B_n^{-1} b_n - 2\langle a_m(x), y \rangle = \\
 &= y^\top B_n^{-1} y - 2 \underbrace{(b_n + B_n a_m(x))^\top}_{\stackrel{\text{def}}{=} d_{mn}^\top(x)} B_n^{-1} y + b_n^\top B_n^{-1} b_n = \\
 &= (y - d_{mn}(x))^\top B_n^{-1} (y - d_{mn}(x)) + b_n^\top B_n^{-1} b_n - d_{mn}^\top(x) B_n^{-1} d_{mn}(x).
 \end{aligned}$$

Afterwards, we rewrite the last two terms:

$$\begin{aligned} b_n^\top B_n^{-1} b_n - d_{mn}^\top(x) B_n^{-1} d_{mn}(x) &= b_n^\top B_n^{-1} b_n - (b_n + B_n a_m(x))^\top B_n^{-1} (b_n + B_n a_m(x)) = \\ b_n^\top B_n^{-1} b_n - b_n^\top B_n^{-1} b_n - b_n^\top B_n^{-1} B_n b_m(x) - a_m^\top(x) B_n B_n^{-1} b_n - a_m^\top(x) B_n B_n^{-1} B_n a_m(x) &= \\ -a_m^\top(x) B_n a_m(x) - 2b_n^\top a_m(x). \end{aligned}$$

Finally, we get

$$\begin{aligned} \exp\left(\frac{f^\theta(y) - c^\theta(x, y)}{\varepsilon}\right) &= \sum_{m=1}^M \sum_{n=1}^N \underbrace{w_n v_m(x) \exp\left(\frac{a_m^\top(x) B_n a_m(x) + 2b_n^\top a_m(x)}{2\varepsilon}\right)}_{\stackrel{\text{def}}{=} z_{mn}(x)} \\ &\cdot \underbrace{\frac{1}{\sqrt{\det(2\pi B_n^{-1})}} \exp\left(-\frac{1}{2}(y - d_{mn}(x))^\top \frac{B_n^{-1}}{\varepsilon} (y - d_{mn}(x))\right)}_{= \mathcal{N}(y | d_{mn}(x), \varepsilon B_n)}, \end{aligned}$$

and thanks to $\int_{\mathcal{Y}} \mathcal{N}(y | d_{mn}(x), \varepsilon B_n) dy = 1$, the normalization constant simplifies to the sum of $z_{mn}(x)$:

$$Z^\theta(x) = \int_{\mathcal{Y}} \exp\left(\frac{f^\theta(y) - c^\theta(x, y)}{\varepsilon}\right) dy = \int_{\mathcal{Y}} \sum_{m=1}^M \sum_{n=1}^N z_{mn}(x) \mathcal{N}(y | d_{mn}(x), \varepsilon B_n) dy = \sum_{m=1}^M \sum_{n=1}^N z_{mn}(x).$$

□

Proof of Proposition 3.2. Combining equations (11), (13) and derivation above, we seamlessly obtain the expression (19) needed for Proposition 3.2. □

D.3. Gradient of our Loss for Energy-Based Modeling

Proof of Proposition A.1. Direct differentiation of (14) gives:

$$\frac{\partial}{\partial \theta} \mathcal{L}(\theta) = \varepsilon^{-1} \mathbb{E}_{x, y \sim \pi^*} \left[\frac{\partial}{\partial \theta} c^\theta(x, y) \right] - \varepsilon^{-1} \mathbb{E}_{y \sim \pi_y^*} \left[\frac{\partial}{\partial \theta} f^\theta(y) \right] + \mathbb{E}_{x \sim \pi_x^*} \left[\frac{\partial}{\partial \theta} \log Z^\theta(x) \right]. \quad (22)$$

Referring to equation (16) for the normalization constant, the last term can be expressed as follows:

$$\begin{aligned} \mathbb{E}_{x \sim \pi_x^*} \left[\frac{1}{Z^\theta(x)} \frac{\partial}{\partial \theta} Z^\theta(x) \right] &= \mathbb{E}_{x \sim \pi_x^*} \left[\frac{1}{Z^\theta(x)} \int_{\mathcal{Y}} \frac{\partial}{\partial \theta} \exp\left(\frac{f^\theta(y) - c^\theta(x, y)}{\varepsilon}\right) dy \right] = \\ \mathbb{E}_{x \sim \pi_x^*} \left[\frac{1}{Z^\theta(x)} \int_{\mathcal{Y}} \frac{\partial}{\partial \theta} (f^\theta(y) - c^\theta(x, y)) \frac{\exp\left(\frac{f^\theta(y) - c^\theta(x, y)}{\varepsilon}\right)}{\varepsilon} dy \right] &= \\ \varepsilon^{-1} \mathbb{E}_{x \sim \pi_x^*} \left[\int_{\mathcal{Y}} \frac{\partial}{\partial \theta} (f^\theta(y) - c^\theta(x, y)) \underbrace{\left\{ \frac{1}{Z^\theta(x)} \exp\left(\frac{f^\theta(y) - c^\theta(x, y)}{\varepsilon}\right) \right\}}_{\pi^\theta(y|x)} dy \right]. \end{aligned}$$

From equation above we obtain:

$$\frac{\partial}{\partial \theta} \mathcal{L}(\theta) = \varepsilon^{-1} \left\{ \mathbb{E}_{x, y \sim \pi^*} \left[\frac{\partial}{\partial \theta} c^\theta(x, y) \right] - \mathbb{E}_{y \sim \pi_y^*} \left[\frac{\partial}{\partial \theta} f^\theta(y) \right] + \mathbb{E}_{x \sim \pi_x^*} \mathbb{E}_{y \sim \pi^\theta(y|x)} \left[\frac{\partial}{\partial \theta} (f^\theta(y) - c^\theta(x, y)) \right] \right\},$$

which concludes the proof. □

D.4. Universal Approximation

Our objective is to set up and use the very general universal approximation result in (Acciaio et al., 2024, Theorem 3.8). Hereinafter, we use the following notation that slightly abuse notation from the main text.

Intra-Section Notation. For any $D \in \mathbb{N}$ we denote the Lebesgue measure on \mathbb{R}^D by λ_D , suppressing the subscript D whenever clear from its context, we use $L^1_+(\mathbb{R}^D)$ to denote the set of Lebesgue integrable (equivalence class of) functions $f : \mathbb{R}^D \rightarrow \mathbb{R}$ for which $\int f(x) \lambda(dx) = 1$ and $f \geq 0$ λ -a.e.; i.e. Lebesgue-densities of probability measures. We use $\mathcal{P}_1^+(\mathbb{R}^D)$ to denote the space of all Borel probability measures on \mathbb{R}^D which are absolutely continuous with respect to λ , metrized by the total variation distance d_{TV} . For any $D \in \mathbb{N}$, we denote the set of $D \times D$ positive-definite matrices by PD_D . Additionally, for any $N \in \mathbb{N}$, we define the N -simplex by $\Delta_N \stackrel{\text{def.}}{=} \{u \in [0, 1]^N : \sum_{n=1}^N u_n = 1\}$. We also denote floor operation for any $x \in \mathbb{R}$ as $\lfloor x \rfloor \stackrel{\text{def.}}{=} \max\{n \in \mathbb{Z} \mid n \leq x\}$.

Lemma D.1 (The Space $(\mathcal{P}_1^+(\mathbb{R}^D), d_{TV})$ is Quantizability by Gaussian Mixtures). *For every $N \in \mathbb{N}$, let $D_N \stackrel{\text{def.}}{=} \frac{N}{2}((D^2 + 3D + 2))$ and define the map*

$$\begin{aligned} GMM_N : \mathbb{R}^{D_N} = \mathbb{R}^N \times \mathbb{R}^{ND} \times \mathbb{R}^{\frac{N}{2}D(D+1)} &\rightarrow \mathcal{P}_1^+(\mathbb{R}^D) \\ (w, \{b_n\}_{n=1}^N, \{B_n\}_{n=1}^N) &\mapsto \sum_{n=1}^N \text{Proj}_{\Delta_N}(w)_n \nu(b_n, \varphi(B_n)) \end{aligned}$$

$\text{Proj}_{\Delta_N} : \mathbb{R}^N \mapsto \Delta_N$ is the ℓ^2 orthogonal projection of \mathbb{R}^N onto the N -simplex Δ_N and $\nu(b_n, \varphi(B_n))$ is the Gaussian measure on \mathbb{R}^D with mean b_n , and non-singular covariance matrix given by $\varphi(B_n)$ where $\varphi : \mathbb{R}^{D(D+1)/2} \rightarrow \text{PD}_D$ is given for each $B \in \mathbb{R}^{D(D+1)/2}$ by

$$\varphi(B) \stackrel{\text{def.}}{=} \exp \left(\begin{pmatrix} B_1 & B_2 & \dots & B_D \\ B_2 & B_3 & \dots & B_{2D-1} \\ \vdots & \ddots & & \vdots \\ B_D & B_{2D-1} & \dots & B_{D(D+1)/2} \end{pmatrix} \right) \quad (23)$$

where \exp is the matrix exponential on the space of $D \times D$ matrices. Then, the family $(GMM_n)_{n=1}^\infty$ is a quantization of $(\mathcal{P}_1^+(\mathbb{R}^D), d_{TV})$ in the sense of (Acciaio et al., 2024, Definition 3.2).

Proof. As implied by (Arabpour et al., 2024, Equation (3.10) in Proposition 7) every Gaussian measure $\mathcal{N}(m, \Sigma) := \mu$ on \mathbb{R}^D with mean $m \in \mathbb{R}^D$ and symmetric positive-definite covariance matrix Σ can be represented as

$$\mu = \mathcal{N}(m, \varphi(X)) \quad (24)$$

for some (unique) vector $X \in \mathbb{R}^{D(D+1)/2}$. Therefore, by definition of a quantization, see (Acciaio et al., 2024, Definition 3.2), it suffices to show that the family of Gaussian mixtures is dense in $(\mathcal{P}_1^+(\mathbb{R}^D), d_{TV})$.

Now, let $\nu \in \mathcal{P}_1^+(\mathbb{R}^D)$ be arbitrary. By definition of $\mathcal{P}_1^+(\mathbb{R}^D)$ the measure ν admits a Radon-Nikodym derivative $f \stackrel{\text{def.}}{=} \frac{D\nu}{D\lambda}$, with respect to the D -dimensional Lebesgue measure λ . Moreover, by the Radon-Nikodym theorem, $f \in L^1_\mu(\mathbb{R}^D)$; and by since μ is a probability measure then $\nu \in L^1_+(\mathbb{R}^D)$.

Since compactly-supported smooth functions are dense in $L^1_+(\mathbb{R}^D)$ then, for every $\varepsilon > 0$, there exists some $\tilde{f} \in C_c^\infty(\mathbb{R}^D)$ with $\tilde{f} \geq 0$ such that

$$\|f - \tilde{f}\|_{L^1(\mathbb{R}^D)} < \frac{\varepsilon}{3}. \quad (25)$$

Since $C_c^\infty(\mathbb{R}^D)$ is dense in $L^1(\mathbb{R}^D)$ then we may without loss of generality re-normalize \tilde{f} to ensure that it integrates to 1.

Since \tilde{f} is compactly supported and approximates f , then (if f is non-zero, which it cannot be as it integrates to 1) then it cannot be analytic, and thus it is non-polynomial. For every $\delta > 0$, let φ_δ denote the density of the D -dimensional Gaussian probability measure with mean 0 and isotropic covariance δI_D (where I_D is the $D \times D$ identity matrix). Therefore, the proof of (Pinkus, 1999, Proposition 3.7) (or any standard mollification argument) shows that we can pick $\delta \stackrel{\text{def.}}{=} \delta(\varepsilon) > 0$ small enough so that the convolution $\tilde{f} \star \varphi_\delta$ satisfies

$$\|\tilde{f} - \tilde{f} \star \varphi_\delta\|_{L^1(\mathbb{R}^D)} < \frac{\varepsilon}{3}. \quad (26)$$

Note that $\tilde{f} \star \varphi_\delta$ is the density of probability measure on \mathbb{R}^D ; namely, the law of a random variable which is the sum of a Gaussian random variance with law $\mathcal{N}(0, \delta I_N)$ and a random variable with law μ . That is, $\tilde{f} \star \varphi_\delta \in L^1_+(\mathbb{R}^D)$. Together (25) and (26) imply that

$$\|f - \tilde{f} \star \varphi_\delta\|_{L^1(\mathbb{R}^D)} < \frac{2\varepsilon}{3}. \quad (27)$$

Recall the definition of the convolution: for each $x \in \mathbb{R}^D$ we have

$$\tilde{f}(x) \star \varphi_\delta \stackrel{\text{def.}}{=} \int_{u \in \mathbb{R}^D} \tilde{f}(u) \varphi_\delta(x - u) \lambda(du). \quad (28)$$

Since $\tilde{f}, \varphi_\delta \in C_c^\infty(\mathbb{R}^D)$ then Lebesgue integral of their product coincides with the Riemann integral of their product; whence, there is an $N \stackrel{\text{def.}}{=} N(\varepsilon) \in \mathbb{N}$ “large enough” so that

$$\left\| \int_{u \in \mathbb{R}^D} \tilde{f}(u) \varphi_\delta(x - u) \lambda(du) - \sum_{n=1}^N \tilde{f}(u_n) \varphi_\delta(x - u_n) \lambda(du) \right\|_{L^1(\mathbb{R}^D)} < \frac{\varepsilon}{3} \quad (29)$$

for some $u_1, \dots, u_N \in \mathbb{N}$. Note that, $\sum_{n=1}^N \tilde{f}(u_n) \varphi_\delta(x - u_n)$ is the law of a Gaussian mixture. Therefore, combining (27) and (29) implies that

$$\left\| f - \sum_{n=1}^N \tilde{f}(u_n) \varphi_\delta(x - u_n) \lambda(du) \right\|_{L^1(\mathbb{R}^D)} < \varepsilon. \quad (30)$$

Finally, recalling that the total variation distance between two measures with integrable Lebesgue density equals the $L^1(\mathbb{R}^D)$ norm of the difference of their densities; yields the conclusion; i.e.

$$d_{TV}(\nu, \hat{\nu}) = \left\| f - \sum_{n=1}^N \tilde{f}(u_n) \varphi_\delta(x - u_n) \lambda(du) \right\|_{L^1(\mathbb{R}^D)} < \varepsilon$$

where $\frac{D\hat{\nu}}{D\lambda} \stackrel{\text{def.}}{=} \sum_{n=1}^N \tilde{f}(u_n) \varphi_\delta(x - u_n) \lambda(du)$. □

Lemma D.2 (The space $(\mathcal{P}_1^+(\mathbb{R}^D), d_{TV})$ is Approximate Simplicial). *Let $\hat{\mathcal{Y}} \stackrel{\text{def.}}{=} \bigcup_{N \in \mathbb{N}} \Delta_N \times [\mathcal{P}_1^+(\mathbb{R}^D)]^N$ and define the map $\eta : \hat{\mathcal{Y}} \mapsto \mathcal{P}_1^+(\mathbb{R}^D)$ by*

$$\eta(w, (r_n)_{n=1}^N) \stackrel{\text{def.}}{=} \sum_{n=1}^N w_n r_n.$$

Then, η is a mixing function, in the sense of (Acciaio et al., 2024, Definition 3.1). Consequentially, $(\mathcal{P}_1^+(\mathbb{R}^D), \eta)$ is approximately simplicial.

Proof. Let $\mathcal{M}^+(\mathbb{R}^D)$ denote the Banach space of all finite signed measures on \mathbb{R}^D with finite total variation norm $\|\cdot\|_{TV}$. Since $\|\cdot - \cdot\|_{TV} = d_{TV}$ when restricted to $\mathcal{P}_1^+(\mathbb{R}^D) \times \mathcal{P}_1^+(\mathbb{R}^D)$ and since $\|\cdot\|_{TV}$ is a norm, then the conclusion follows from (Acciaio et al., 2024, Example 5.1) and since $\mathcal{P}_1^+(\mathbb{R}^D)$ is a convex subset of $\mathcal{M}^+(\mathbb{R}^D)$. □

Together, Lemmata D.1 and D.2 imply that $(\mathcal{P}_1^+(\mathbb{R}^D), d_{TV}, \eta, Q)$ is a QAS space in the sense of (Acciaio et al., 2024, Definition 3.4), where $Q \stackrel{\text{def.}}{=} (GMM_M)_{M \in \mathbb{N}}$. Consequentially, the following is a geometric attention mechanism in the sense of (Acciaio et al., 2024, Definition 3.5)

$$\begin{aligned} \hat{\eta} : \bigcup_{N \in \mathbb{N}} \Delta_N \times \mathbb{R}^{N \times D_M} &\rightarrow \mathcal{P}_1^+(\mathbb{R}^D) \\ \left(w, (v_m, (b_{mn})_{n=1}^N, (B_{mn})_{n=1}^N)_{m=1}^M \right) &\mapsto \sum_{n=1}^N w_n \sum_{m=1}^M \text{Proj}_{\Delta_M}(v_m)_n \nu(b_{mn}, \varphi(B_{mn})). \end{aligned}$$

Before presenting our main theorem, we first introduce several definitions of activation functions that will be used in the theorem. These definitions, which are essential for completeness, are taken from (Acciaio et al., 2024, Definitions 2.2-2.4).

Definition D.3 (Trainable Activation Function: Singular-ReLU Type). A trainable activation function σ is of *ReLU+Step* type if

$$\sigma_\alpha : \mathbb{R} \ni x \mapsto \alpha_1 \max\{x, \alpha_2 x\} + (1 - \alpha_1) [x] \in \mathbb{R}$$

Definition D.4 (Trainable Activation Function: Smooth-ReLU Type). A trainable activation function σ is of *smooth non-polynomial* type if there is a non-polynomial $\sigma^* \in C_c^\infty(\mathbb{R})$, for which

$$\sigma_\alpha : \mathbb{R} \ni x \mapsto \alpha_1 \max\{x, \alpha_2 x\} + (1 - \alpha_1) \sigma^*(x) \in \mathbb{R}$$

Definition D.5 (Classical Activation Function). Let $\sigma^* \in C_c^\infty(\mathbb{R})$ be non-affine and such that there is some $x \in \mathbb{R}$ at which σ is differentiable and has non-zero derivative. Then σ is a classical regular activation function if, for every $\alpha \in \mathbb{R}^2$, $\sigma_\alpha = \sigma^*$.

Further in the text, we assume that activation functions are applied element-wise to each vector $x \in \mathbb{R}^D$. We are now ready to prove the first part of our approximation theorem.

Proposition D.6 (Deep Gaussian Mixtures are Universal Conditional Distributions in the TV Distance). Let $\pi : (\mathbb{R}^D, \|\cdot\|_2) \rightarrow (\mathcal{P}_1^+(\mathbb{R}^D), d_{TV})$ be Hölder. Then, for every compact subset $K \subseteq \mathbb{R}^D$, every approximation error $\varepsilon > 0$ there exists $M, N \in \mathbb{N}$ and a MLP $\hat{f} : \mathbb{R}^D \mapsto \mathbb{R}^{N \times ND_M}$ with activations as in Definitions D.3, D.4, D.5 such that the (non-degenerate) Gaussian-mixture valued map

$$\hat{\pi}(\cdot|x) \stackrel{\text{def.}}{=} \hat{\eta} \circ \hat{f}(x)$$

satisfies the uniform estimate

$$\max_{x \in K} d_{TV}(\hat{\pi}(\cdot|x) \| \pi(\cdot|x)) < \varepsilon.$$

Proof. Since Lemmata D.2 and D.1 imply that $(\mathcal{P}_1^+(\mathbb{R}^D), d_{TV}, \eta, Q)$, is a QAS space in the sense of (Acciaio et al., 2024, Definition 3.4), then the conclusion follows directly from (Acciaio et al., 2024, Theorem 3.8). \square

Since many of our results are formulated in the Kullback-Leibler divergence, then our desired guarantee is obtained only under some additional mild regularity requirements of the target conditional distribution $\hat{\pi}$ being approximated.

Assumption D.7 (Regularity of Conditional Distribution). Let $\pi : (\mathbb{R}^D, \|\cdot\|_2) \rightarrow (\mathcal{P}_1^+(\mathbb{R}^D), d_{TV})$ be Hölder, for each $x \in \mathbb{R}^D$, $\pi(\cdot|x)$ is absolutely continuous with respect to the Lebesgue measure λ on \mathbb{R}^D , and suppose that there exist some $0 < \delta \leq \Delta$ such that its conditional Lebesgue density satisfies

$$\delta \leq \frac{d\pi(\cdot|x)}{d\lambda} \leq \Delta \quad \text{for all } x \in \mathbb{R}^D. \quad (31)$$

Theorem D.8 (Deep Gaussian Mixtures are Universal Conditional Distributions). Suppose that π satisfies Assumption D.7. Then, for every compact subset $K \subseteq \mathbb{R}^D$, every approximation error $\varepsilon > 0$ there exists $M, N \in \mathbb{N}$ such that: for each $m = 1, \dots, M$ and $n = 1, \dots, N$ there exist MLPs: $a_m : \mathbb{R}^{D_x} \mapsto \mathbb{R}^{D_y}$, $v_m : \mathbb{R}^{D_x} \mapsto \mathbb{R}^M$ with ReLU activation functions and w_n, B_n learnable parameters such that the (non-degenerate) Gaussian-mixture valued map

$$\hat{\pi}(\cdot|x) \stackrel{\text{def.}}{=} \sum_{n=1}^N \sum_{m=1}^M z_{mn}(x) \nu(d_{mn}(x), \varphi(D_{mn}(x)))$$

satisfies the uniform estimate

$$\max_{x \in K} d_{TV}(\pi(\cdot|x), \hat{\pi}(\cdot|x)) < \varepsilon. \quad (32)$$

If, moreover, $\hat{\pi}$ also satisfies (31) (with $\hat{\pi}$ in place of π) then additionally

$$\max_{x \in K} \text{KL}(\pi(\cdot|x), \hat{\pi}(\cdot|x)) \in \mathcal{O}(\varepsilon), \quad (33)$$

where \mathcal{O} hides a constant independent of ε and of the dimension D .

The proof of Theorem D.8 makes use of the *symmetrized Kullback-Leibler divergence* KL_{sym} is defined for any two $\alpha, \beta \in \mathcal{P}(\mathbb{R}^D)$ by $\text{KL}_{sym}(\mu, \nu) \stackrel{\text{def.}}{=} \text{KL}(\alpha\|\beta) + \text{KL}(\beta\|\alpha)$; note, if $\text{KL}_{sym}(\alpha, \beta) = 0$ then $\text{KL}_{sym}(\alpha\|\beta) = 0$. We now prove our main approximation guarantee.

Proof of Theorem D.8. To simplify the explanation of our first claim, we provide the expression for $\hat{\pi}(y|x)$ from (19):

$$\hat{\pi}(y|x) = \sum_{n=1}^N w_n \sum_{m=1}^M v_m(x) \exp\left(\frac{a_m^\top(x) B_n a_m(x) + 2b_n^\top a_m(x)}{2\varepsilon}\right) \mathcal{N}(y | d_{mn}(x), \varepsilon B_n)$$

Thanks to the wide variety of activation functions available from Definitions D.3, D.4, D.5, we can construct the map \hat{f} and directly apply Proposition D.6. This completes the proof of the first claim.

Under Assumption D.7, $\pi(\cdot|x)$ and $\hat{\pi}(\cdot|x)$ are equivalent to the D -dimensional Lebesgue measure λ . Consequentially,

$$\pi(\cdot|x) \ll \hat{\pi}(\cdot|x)$$

for all $x \in \mathbb{R}^{D_x}$. Therefore, the Radon-Nikodym derivative $\frac{\hat{\pi}(\cdot|x)}{\pi(\cdot|x)}$ is a well-defined element of $L^1(\mathbb{R}^{D_x})$, for each $x \in \mathbb{R}^{D_x}$; furthermore, we have

$$\frac{\pi(\cdot|x)}{\hat{\pi}(\cdot|x)} = \frac{\pi(\cdot|x)}{d\lambda} \frac{d\lambda}{\hat{\pi}(\cdot|x)}. \quad (34)$$

Again, leaning on Assumption 31 and the Hölder inequality, we deduce that

$$\begin{aligned} \sup_{a \in \mathbb{R}^D} \left| \frac{\pi(\cdot|x)}{\hat{\pi}(\cdot|x)}(a) \right| &= \sup_{a \in \mathbb{R}^D} \left| \frac{\pi(\cdot|x)}{d\lambda}(a) \frac{d\lambda}{\hat{\pi}(\cdot|x)}(a) \right| \\ &\leq \sup_{a \in \mathbb{R}^D} \left| \frac{\pi(\cdot|x)}{d\lambda}(a) \right| \sup_{a \in \mathbb{R}^D} \left| \frac{d\lambda}{\hat{\pi}(\cdot|x)}(a) \right| \\ &\leq \sup_{a \in \mathbb{R}^D} \left| \frac{\pi(\cdot|x)}{d\lambda}(a) \right| \frac{1}{\delta} \\ &\leq \frac{\Delta}{\delta} \end{aligned} \quad (35)$$

where the final inequality held under the assumption that $\hat{\pi}$ also satisfies Assumption 31. Importantly, we emphasize that the right-hand side of (35) held *independently* of $x \in \mathbb{R}^{D_x}$ (“which we are conditioning on”). A nearly identical estimate holds for the corresponding lower-bound. Therefore, we may apply (Sason, 2015, Theorem 1) to deduce that: there exists a constant $C > 0$ (independent of $x \in \mathbb{R}^{D_x}$ and depending only on the quantities $\frac{\Delta}{\delta}$ and $\frac{\delta}{\Delta}$; thus only on δ, Δ) such that: for each $x \in \mathbb{R}^{D_x}$

$$\text{KL}(\pi(\cdot|x), \hat{\pi}(\cdot|x)) \leq C d_{TV}(\pi(\cdot|x), \hat{\pi}(\cdot|x)). \quad (36)$$

The conclusion now follows, since the right-hand side of (36) was controllable by the first statement; i.e. since (32) held we have

$$\text{KL}(\pi(\cdot|x), \hat{\pi}(\cdot|x)) \leq C d_{TV}(\pi(\cdot|x), \hat{\pi}(\cdot|x)) \leq C\varepsilon. \quad (37)$$

A nearly identical derivation shows that

$$\text{KL}(\hat{\pi}(\cdot|x), \pi(\cdot|x)) \leq C\varepsilon. \quad (38)$$

Combining (37) and (38) yields the following bound

$$\max_{x \in K} \text{KL}_{sym}(\pi(\cdot|x), \hat{\pi}(\cdot|x)) \in \mathcal{O}(\varepsilon). \quad (39)$$

Since $\text{KL}(\alpha||\beta) \leq \text{KL}_{sym}(\alpha, \beta)$ for every pair of Borel probability measures α and β on \mathbb{R}^{D_x} then (39) implies (33). \square